Shape Selective Conversion of Methanol to Hydrocarbons over Uni-Dimensional 10-ring Zeolites

Dissertation for the degree of

Philosophiae Doctor

Shewangizaw Teketel Forsido

DEPARTMENT OF CHEMISTRY

Faculty of mathematics and natural sciences

UNIVERSITY OF OSLO

December 2012

Series of dissertations submitted to the
Faculty of Mathematics and Natural Sciences, University of Oslo
No. 1321

ISSN 1501-7710

Cover: Inger Sandved Anfinsen.
Printed in Norway: AIT Oslo AS.

Produced in co-operation with Akademika publishing.
The thesis is produced by Akademika publishing merely in connection with the thesis defence. Kindly direct all inquiries regarding the thesis to the copyright holder or the unit which grants the doctorate.

Preface

This Ph.D. thesis is submitted to the Department of Chemistry, Faculty of Mathematics and Natural Sciences, University of Oslo (UiO). My employment at UiO was from August 2009 to February 2013, a total of six months of the time was spent at the laboratories of Haldor Tøpsoe A/S, Denmark. The work was financed by the Innovative Natural Gas Processes and Products (*in*GAP), Centre of Research-based Innovation, which receives financial support from the Norwegian Research Council under Contract No. 174893.

Associate Professor Stian Svelle (UiO) has been my principal supervisor. Professor Unni Olsbye (UiO), Professor Karl Petter Lillerud (UiO) and Doctor Pablo Beato (Haldor Topsøe) were my subsidiary supervisors. Stian is greatly acknowledged for his close guidance and fruitful discussions throughout the Ph.D. work. Pablo is greatly acknowledged for his guidance and great time during my industrial traineeship in Denmark. Unni and Karl Petter are greatly acknowledged for their contribution through fruitful discussions.

The work behind paper I was carried out during my master degree, under supervision of Professor Unni Olsbye. However, since it is relevant for the Ph.D. work, I have included it in this thesis.

I would like to thank my colleagues at the catalysis group for the very nice working environment. I want to particularly mention Wegard Skistad for our discussions, and Marius W. Erichsen for reading the draft of this thesis. Special thanks to people outside the catalysis group: Marit, Endrias, Stian and friend in OiC for the good company. Finally, my parents Ato Teketel Forsido and W/O Zenebech Banjaw are greatly acknowledged for their encouragement and support.

Shewangizaw Teketel Forsido

December, 2012

Table of Contents

List of papers **III**

The author's contribution IV

Conference contributions V

Patent application V

Related papers VI

1. Introduction **1**

1.1. Catalysis in general 1

1.2. Zeolites 2

1.3. Zeolites as acid catalysts 6

1.4. Catalysts employed in this work 8

2. Methanol to Hydrocarbons (MTH) **13**

2.1. Historical development 13

2.2. Reaction mechanism 15

3. Experimental **21**

3.1. Catalyst synthesis and preparation 21

3.1. Catalyst characterization 24

3.2. Catalytic tests 26

3.3. Isotope labeling studies 30

4. This work **35**

4.1. Scope 35

4.2. Summary of results 36

4.3. Main conclusions 53

Suggestions for further work **55**

References **57**

Appendix **65**

List of papers

Paper I: *Shape-Selective Conversion of Methanol to Hydrocarbons Over 10-Ring Unidirectional-Channel Acidic H-ZSM-22*. S. Teketel, S. Svelle, K. P. Lillerud, U. Olsbye. *ChemCatChem* 1 (2009) 78-81

Paper II: *Selectivity Control through Fundamental Mechanistic Insight in the Conversion of Methanol to Hydrocarbons over Zeolites.* S. Teketel, U. Olsbye, K. P. Lillerud, P. Beato, S. Svelle. *Microporous Mesoporous Mater.* 136 (2010) 33-41.

Paper III: *Shape Selectivity in the Conversion of Methanol to Hydrocarbons: The Catalytic Performance of One-Dimensional 10-Ring Zeolites: ZSM-22, ZSM-23, ZSM-48, and EU-1*. S. Teketel, W. Skistad, S. Benard, U. Olsbye, K. P. Lillerud, P. Beato, S. Svelle. *ACS Catal.* 2 (2012) 26-37

Paper IV: *Morphology Induced Shape Selectivity in Zeolite Catalysis*. S. Teketel, L. F. Lundegaard, U. Olsbye, K. P. Lillerud, P. Beato, S. Svelle. *To be submitted (*2012).

Paper V: *Co-conversion of Methanol and Light Alkenes to Hydrocarbons over Acidic Zeolite Catalyst H-ZSM-22: Simulated Recycle of Non-Gasoline Products.* S. Teketel, U. Olsbye, K. P. Lillerud, P. Beato, S. Svelle. *In Preparation,* (2012).

The author's contribution

Paper I: The author synthesized, characterized the zeolite, and performed all the catalytic tests. The author contributed to the planning of the experiments, interpretation of the results and preparation of the manuscript.

Paper II: The author synthesized, characterized the zeolite, and performed all the catalytic tests. The author contributed to the planning of the experiments, interpretation of the results and preparation of the manuscript.

Paper III: The author contributed to the synthesis and characterization of the zeolites, and performed all the catalytic tests. The author was involved in the planning of the experiments, interpretation of the results and preparation of the manuscript. EU-1 zeolite was synthesized by Wegard Skistad, and ZSM-48 was synthesized by Wegard Skistad in collaboration with Sandrine Benard.

Paper IV: The author synthesized, characterized the zeolite and performed all the catalytic tests. The author contributed to the planning of the experiments, interpretation of the results and preparation of the manuscript. TEM and XRD analyses of the catalyst were performed by Lars F. Lundegaard.

Paper V: The author has performed all the catalytic tests. The author contributed to the planning of the experiments, interpretation of the results, and preparation of the manuscript.

Conference contributions

I. *Conversion of Methanol to Hydrocarbons over 10-ring Unidirectional Acidic H-ZSM-22.* S. Teketel, S. Svelle, K. P. Lillerud, P. Beato, U. Olsbye. *Norwegian Catalysis Symposium*, Trondheim, Norway, 2009/11/30 (**Oral presentation**)

II. *Production of Non-Aromatic Gasoline from Methanol over Unidirectional 10-ring Zeolite Catalysts.* S. Teketel, W. Skistad, S. Benard, U. Olsbye, K. P. Lillerud, P. Beato, S. Svelle. *EuropaCat,* Glasgow, Scotland 2011/08/28 (**Poster presentation**)

III. *Shape Selectivity in the Conversion of Methanol to Hydrocarbons: the Catalytic Performance of 1D 10-ring Zeolite: ZSM-22, ZSM-23, ZSM-48 and EU-1*. S. Teketel, W. Skistad, S. Benard, U. Olsbye, K. P. Lillerud, P. Beato, S. Svelle. *Norwegian Catalysis Symposium,* Lillestrøm, Norway, 2011/09/28 (**Oral presentation**)

Patent application

I. *Catalyst for the Conversion of Oxygenates to Olefins and a Process for Preparing Said Catalyst.* S. Teketel, S. Svelle and P. Beato, *Danish Patent Office*, Reference number: 1037 DK BECH/ANKR, Copenhagen, Denmark, 2011/07/22.

Related papers

I. *Interplay Between Nanoscale Reactivity and Bulk Performance of H-ZSM-5 Catalysts during the Methanol to Hydrocarbons Reaction*. L. R. Aramburo, S. Teketel, S. Svelle, S. R. Bare, B. Arstad, H. W. Zandbergen, U. Olsbye, F. M. F. de Groot, B. M. Weckhuysen. Submitted to *J. Catal.* (2012).

II. *Large Zeolite H-*ZSM-5 *Crystals as Models for the Methanol to Hydrocarbons Process: Bridging the Gap between Individual Crystals and Powdered Catyalysts,* J. P. Hafmann, D. Mores, L. R. Aramburo, S. Teketel, M. Rohnke, J. Janek, U. Olsbye, B. M. Weckhuysen. *Submitted to Chem. A Rurop. J.* (2012)

III. *Single-Event MicroKinetics (SEMK) for Methanol to Hydrocarbons (MTH) on H-ZSM-23,* P. Kumar, J. W. Thybaut, S. Teketel, S. Svelle, U. Olsbye, P. Beato, G. B. Marin. Submitted to *Catal. Today*, (2012).

IV. *Combined Operando Spectroscopy and Ex-situ Chemical Analysis Tools for Mechanistic Investigations of the Methanol to Hydrocarbon Reaction,* S. Teketel, F. Bonino, W. Skistad, U. Olsbye, K. P. Lillerud, S. Bordiga, S. Svelle, P. Beat. Submitted to *Catal. Today*, (2012).

1. Introduction

1.1. Catalysis in general

In order for a chemical reaction to occur, the reactant molecules must overcome an energy barrier. A catalyst is a substance that accelerates the progress of a chemical reaction towards equilibrium, and allows the reaction to occur with a low energy barrier. A catalyst does not change the thermodynamics (energy difference between starting materials and products) and the equilibrium concentrations of a reaction. Figure 1.1 displays potential energy diagrams of catalytic and non-catalytic reactions. The non-catalytic reaction path goes through a much higher energy barrier, full curve [1].

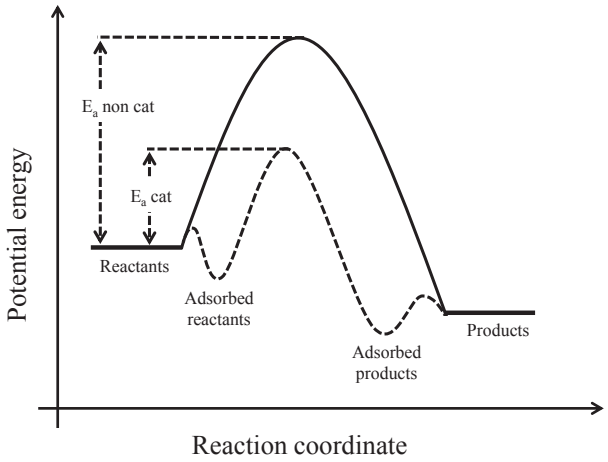

Figure 1.1: Potential energy diagram for non-catalytic path (full curve) catalytic (dotted curve).

The catalytic path is more complex but thermodynamically favorable, dotted curve. It involves adsorption of the reactants on to the active sites, reactions leading to product formation, and finally desorption of the product from the catalyst. In addition to lowering of the energy barrier of chemical reactions, catalysts increase the number of collisions between reactant molecules by offering adsorption sites [1]. Catalysis is divided in to three sub-disciplines: homogeneous, heterogeneous and biocatalysis (enzymatic) catalysis. In homogeneous catalysis, reactants, products and the catalyst are in one phase, usually in a liquid phase. In heterogeneous catalysis, the reactant, products and the catalyst are in different phases. Usually, the catalyst is a solid while the reactant and product are gases or liquids.

Biocatalysis is based on enzymes, proteins which are highly specific to certain substrates and products.

In the last century catalysis was aimed at increasing turnover rates, but during the 20th century, catalysis evolved into understanding and controlling selectivity [2-4]. Therefore in this century, in addition to increased turnover rates, catalysts are required to provide selectivity towards desired products. In such catalytic processes, raw materials are used more efficiently and waste production is minimized. Most chemical industries rely on catalysts and about 85-90 % of all petrochemical products are made in catalytic processes [5].

1.2. Zeolites

Zeolites are crystalline aluminosilicates with a three-dimensional framework that consists of nanometer-sized channels and cages, giving a high porosity and a large surface area to the material [6]. The three-dimensional framework of zeolites is constructed from corner shared tetrahedral (T-atoms) of silicon and aluminum, bridged with oxygen atoms. The dimensions of zeolite channels, channel intersections and/or cages are typically less than 2 nm. The International Union of Pure and Applied Chemistry (IUPAC) classifies porous materials as mirocoporous, mesoporous and macroporous based on sizes < 2 nm, 2-50 nm and > 50 nm respectively [7], therefore zeolites are referred to as microporous materials. Figure 1.2 illustrates examples of selected zeolite structures along with their pore systems. The zeolite pore size is mainly determined by the number of T-atoms defining the entrance (ring-size) to the interior of the crystal, for example in Figure 1.2 the pore size of ZSM-22 (10-ring) is smaller than that of ZSM-12 (12-ring). Accordingly, zeolites are classified as having small, medium, large, and extra-large pore structures for pore windows delimited by 8, 10, 12, and more than 12 T-atoms, respectively [8]. The pores in zeolites can be one-dimensional (Figure 1.2, ZSM-12 and ZSM-22), two-dimensional (for example MCM-22 [9]), or three-dimensional (Figure 1.2, ZSM-5 and Faujasite). The pore sizes of zeolites are in the range of the molecular diameters of organic compounds, and only molecules with smaller free diameter than the zeolite pores can have access to the interior of the zeolite crystal. Due to such ability to sort molecules based on sizes, zeolites are often described as molecular sieves [10].

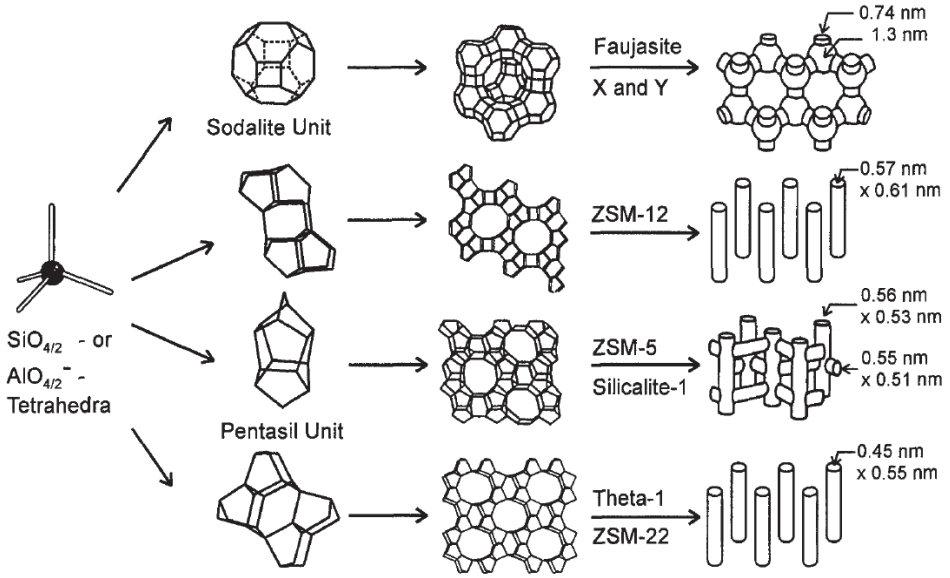

Figure 1.2: Structures of zeolites (from top to bottom: faujasite or zeolite X, Y; zeolite ZSM-12; zeolite ZSM-5 or silicalite-1; zeolite ZSM-22) and their micropore system. Adapted from Ref. [11]

The first naturally occurring zeolite was recognized in 1756 by a Swedish mineralogist, Cronstedt [10]. He named it "zeolite" from the Greek words "zein" (boiling) and "lithos" (stone) because the new material released large amounts of steam and water upon heating. Currently there are nearly 200 zeolites maintained in the database of the International Zeolite Association (IZA) [9]. All zeolite structures are given a three capital letters code, following the rule set by an IUPAC Commission on Zeolite Nomenclature [12, 13]. About one fifth of the zeolites in the IZA database are naturally occurring, and the rest are synthetic zeolites made in laboratories. Furthermore, computer prediction of hypothetical zeolites shows several million possible structures, of which 450000 are potentially stable when their calculated lattice energies are compared with those of known zeolite structures [8]. Hypothetical zeolite structures are also maintained in an online databases [14, 15].

The synthesis of zeolites is usually carried out under hydrothermal conditions, from sources of silicon, aluminum dissolved in aqueous solution of alkali hydroxide and structure directing agent (SDA), illustrated in Figure 1.3. Zeolites are metastable and the final synthesis product is determined by factors such as nature and concentrations of reactants and synthesis conditions (temperature, crystallization time, and pH). The hydrothermal synthesis of zeolites is often carried out in autoclave at elevated temperature and autogenous pressure. Crystallization from solution generally occurs via the sequential steps of nucleation of the

phase(s), dictated by the composition of the solution, followed by growth of the nuclei to larger sizes by incorporation of solute from the solution [16]. The final crystal size is a function of the ratio between rate of nucleation and rate of growth of the nuclei [17]. The zeolite crystallization process is dependent on a number of parameters such as: ageing of the synthesis gel [18], solubility of silicon [19], crystallization temperature [20], and addition of seed crystals [21].

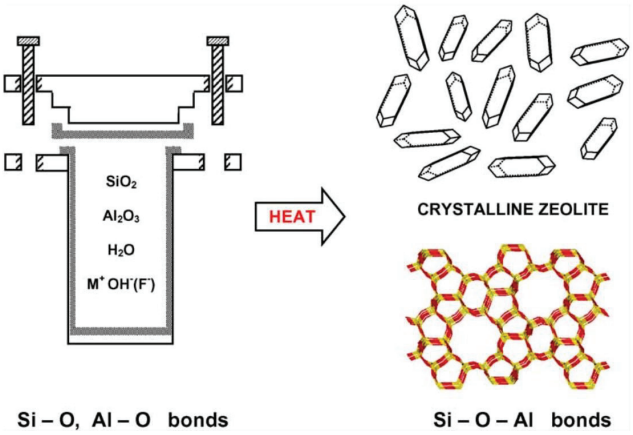

Figure 1.3**:** Illustration of hydrothermal zeolite synthesis. Adapted from Ref. [22]

Crystal sizes play important roles in application of zeolites as catalyst. For example, catalyst effectiveness is larger for smaller crystals, but filtration and recovery of very small crystals can be practically a challenge. Shape selective catalysis requires larger crystals (see section 1.3.), but deactivation can be more severe and regeneration of used catalyst can be more difficult for larger crystal [17].

Zeolites have wide spread applications such as catalysts in oil refineries, gas separation, and ion exchange [23-26]. However considering market values, the catalytic application of zeolites is the most important [27]. The possibility of generating functionality within the zeolite pores by introducing hetroatoms into the framework and/or extra framework make them attractive for wide range of applications. Such functionality may have acid, base, redox or bifunctional properties, and act as active site to catalyze numerous reactions [28]. The wide application of zeolites is due to their physical properties such as: high surface area, temperature stability, molecular sieve property, or ion-exchange ability. This thesis strictly deals application of zeolites as acid catalysts.

The name zeolite is restricted to frameworks constructed from silicon and aluminum as central atoms (T-atoms). There are other Zeotype materials with similar framework construction as zeolites but different T-atom. Some of this classes of materials are: SAPO (in which the T-atoms are Si, Al, and P), $AlPO_4$ (in which the T-atoms are Al, and P), MeAPO (in which the T-atoms are metal cation, Al, and P), and MeSAPO (in which the T-atoms are metal cation, Si, Al, and P).

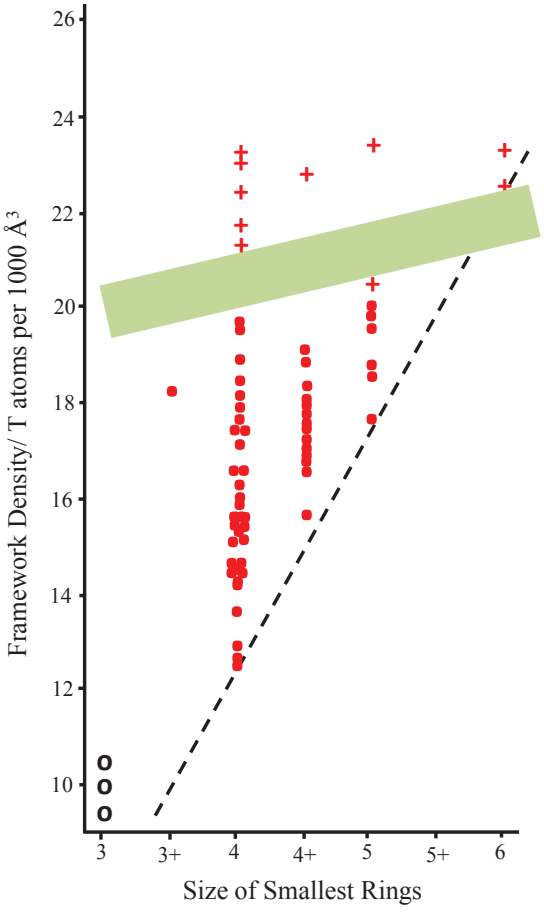

Figure 1.4: Distribution of framework density (FD) versus size of smallest ring in the framework. Framework types: a) + dense framework; ● zeolite; ○ hypothetical. Adapted from Ref. [8], similar figures can be found in Refs. [12, 29]

Zeolites and Zeotype materials can be distinguished from denser materials of similar type based on their framework density (FD), the number of T-atoms per 1000 $Å^3$. For zeolites and Zeotype materials values in the range 12.1 T-atoms to around 20.6 T-atoms per 1000 $Å^3$ are observed, while for dense materials the observed values of at least 20 T-atoms per 1000

$Å^3$ [12]. Figure 1.4 displays distribution of framework density versus size of smallest ring in the framework. The range of the observed FD values depends on the type and relative number of the smallest rings in the tetrahedral networks, and the frameworks of the lowest density are those with a maximum number of 4-rings [29]. Furthermore, there is a clear gap in the FD values between zeolites and dense frameworks, and this also depends on the type of the smallest rings present.

1.3. Zeolites as acid catalysts

The first use of zeolites as acid catalysts goes back to 1959 when zeolite Y was used as an isomerization catalyst by Union Carbide. Later in 1962, incorporation of relatively small amounts of the zeolite X as a promoter greatly improved the performance of silica/alumina or silica/clay based catalysts for petroleum cracking (i.e. the production of petrol from crude oil) [10]. The application of acid zeolites within refineries has been responsible for the huge amount of money and time that has been invested in zeolite research.

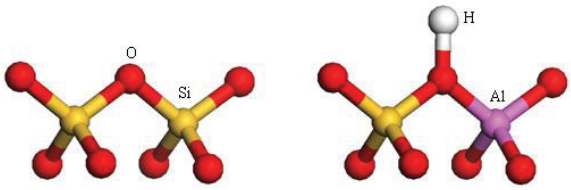

Figure 1.5: Illustration of Brønsted acid site in zeolite

The acidity required for acid catalysis can be introduced in zeolites by isomorphous substitution of silicon (Si) by aluminum (Al) in the framework, illustrated in Figure 1.5. A zeolite framework constructed from silicon and oxygen atoms only is neutral, but replacing tetravalent Si with trivalent Al creates a negative charge on the framework. All such zeolites are neutralized by ion-exchangable cations such as K^+ and Na^+ that reside inside zeolites pores. If the cations are ion-exchanged with protons, Brønsted sites with high acid strength are formed within the zeolite framework [30]. Protonated zeolites were considered as super acids, but studies have shown that the sites are weaker than 100 % sulfuric acid, which is the measure of super acidity [31]. To this day, zeolites remain inevitable in hydrocarbon conversion reactions in oil refineries as shape selective catalysts [28, 32]. One third of all gasoline is produced via zeolite based catalytic cracking of vacuum gas oil and similar heavy feedstocks [5, 33].

Shape selectivity: One of the most important applications of zeolites is shape selective catalysis. The concept of shape selectivity in zeolite catalysis was introduced in the 1950s: the chemical transformation of molecules depends on the space offered by the zeolite [6]. Some of our day to day substances such as gasoline or plastic bottles have experienced the effect of shape selectivity [6].

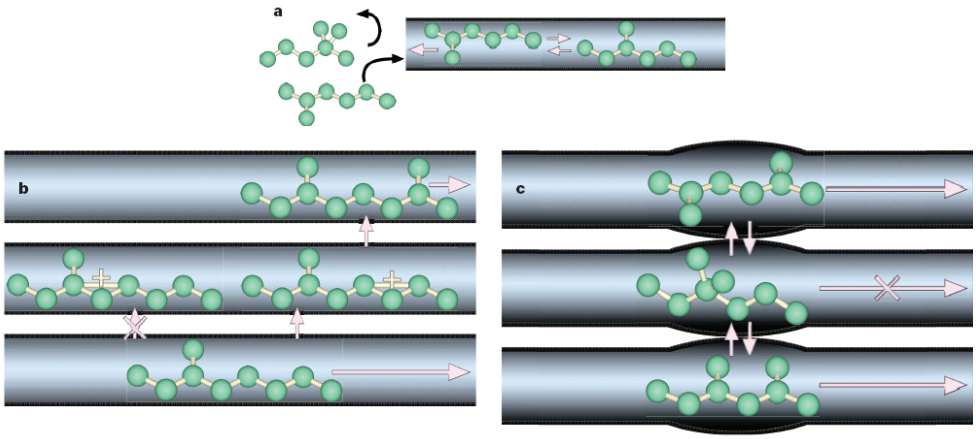

Figure 1.6: Illustration of zeolite shape selectivity a) reactant selectivity, b) restricted transition state selectivity and c) product selectivity. Adopted from Ref. [6].

Shape selectivity in zeolites is described on the bases of mass transport limitations or transition state control of reactions. This provide an adequate rationalization of well know reactant selectivity (Figure 1.6a), restricted transition state selectivity (Figure 1.6b) and product selectivity (Figure 1.6c).

- *Reactant shape selectivity* is encountered when bulkier molecules in a reactant mixture are excluded from reaching the active sites within the zeolite crystal [34]. Only molecules that are smaller than the pore opening of the zeolite can be converted over the active sites.
- *Restricted transition state selectivity* is encountered in chemical reactions that involve transition states which are too bulky to be accommodated inside the zeolite pores [35]. In this case, products are formed from reactions with intermediates that can fit inside the pores of the zeolite. In restricted transition state selectivity, neither reactants nor potential products are hindered from diffusing in or out of the zeolite crystal [35].
- *Product shape selectivity* is encountered when certain product molecules are too big to diffuse intact out of the zeolite pores [34]. Some zeolite structures have cavities which

allow formation of both small and bulky products. However, the apertures are small, and the bulky product molecules must undergo further reactions to smaller molecules to leave the zeolite crystal.

In general, both reactant and product shape selectivities occur due to mass transfer limitations. In reactant shape selectivity molecules that diffuse sufficiently fast to the active sites will be converted. In contrast, in product shape selectivity molecules with high mass transport limitations remain in the adsorbed phase and continue to react for a longer period of time than other less mass transfer limited species. Therefore, both reactant and product shape selectivities are affected by crystal sizes, whereas restricted transition state selectivity does not depend on crystal size [35].

Shape selective catalysis has a number of advantages over non-shape selective catalysis. In shape selective catalysis smaller amounts of by-products are formed, meaning that the amount of desired products is increased. This makes processes based on shape selective catalysts more environmentally friendly. Furthermore, shape selective catalysis reduces costs related to the separation and disposal of waste products [35].

1.4. Catalysts employed in this work

The catalysts employed in this work are outlined in Table 1.1.

Table 1.1: List and descriptions of catalysts employed in this work

Topology (Material)	Channel/ring	Main channel	Side pocket or cage	Max. diameter of a sphere that can be included inside the largest opening[a] [9]
TON (ZSM-22)	1D/10 ring	4.6 × 5.7 Å	None	5.71 Å
MTT (ZSM-23)	1D/10 ring	4.5 × 5.2 Å	Very small	6.19 Å
*MRE (ZSM-48)	1D/10 ring	5.3 × 5.6 Å	None	6.36 Å
EUO (EU-1)	1D/10 ring	4.1 × 5.4 Å	6.8 × 5.8 × 8.1 Å	7.00 Å
SZR (SUZ-4)	3D/8 and 10 rings	4.8 × 3.2 Å (8) 4.1 × 5.2 Å (10)	None	6.27 Å
CHA (SAPO-34)	3D/8 ring	3.8 × 3.8 Å	7.37 Å	7.37 Å
MFI (ZSM-5)	3D/10 ring	5.3 × 5.5 Å & 5.4 × 5.6 Å	None	6.36 Å
*BEA (Beta)	3D/12 ring	7.3 × 7.1 Å & 5.6 × 5.6 Å	None	6.68 Å

*Disordered structures, [a] Channel, cage or channel intersections

The channel (pore) sizes described in this thesis are based upon atomic coordinates of the *Type material* and an oxygen radius of 1.35 Å, as described by Meier et al. [12]. The crystallographic free diameters of the channels (interatomic distance vectors) are presented in Ångstrom (10^{-10} meter) units. Four one-dimensional 10-ring zeolites, ZSM-22, ZSM-23, EU-1 and ZSM-48, and one three-dimensional zeolite SUZ-4 are studied. The catalytic performance of the materials studied in this thesis is compared with three well known methanol to hydrocarbon (MTH) (see Chapter 2) catalysts, namely SAPO-34, ZSM-5 and Beta [36]. All the catalysts are briefly presented below. The pores of the one-dimensional 10-ring zeolites and SUZ-4 are illustrated using Figures 1.7 to 1.11.

TON (ZSM-22): ZSM-22 is a one-dimensional 10-ring zeolite. The 10-ring channels of the material are elliptical and slightly zigzag in shape, and have dimensions 5.7 × 4.6 Å [9, 12], illustrated in Figure 1.7. The maximum diameter of a sphere that can be included in the channels of ZSM-22 is 5.71 Å [9].

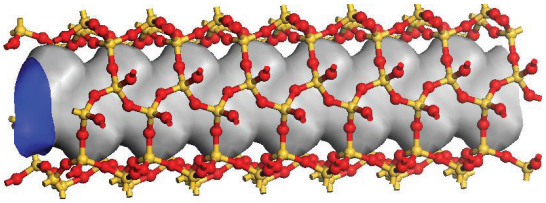

Figure 1.7: Illustration of the channel systems of ZSM-22 zeolite

MTT (ZSM-23): ZSM-23 is a one-dimensional 10-ring zeolite with teardrop-shaped channels of 5.2 × 4.5 Å dimensions [12]. The 10-ring channels of ZSM-23 can be described as having very small pore extensions or side pockets, illustrated in Figure 1.8. The maximum diameter of a sphere that can be included in the channels of ZSM-23 is 6.19 Å [9].

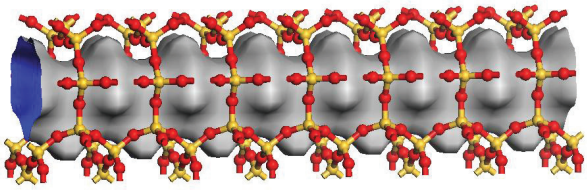

Figure 1.8: Illustration of the channel systems of ZSM-23 zeolite

***MRE (ZSM-48):** ZSM-48 is a disordered one-dimensional 10-ring zeolite, with nearly symmetrical straight channels, illustrated in Figure 1.9. The channels are 5.3 × 5.6 Å in

dimension [37], and the maximum diameter of a sphere that can be included in the channels is 6.36 Å [9].

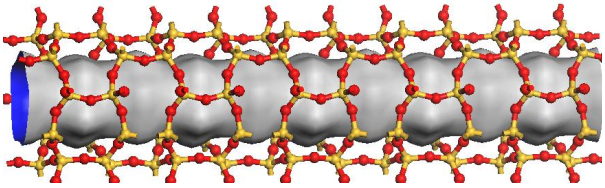

Figure 1.9: Illustration of the channel systems of ZSM-48 zeolite

EUO (EU-1): EU-1 is a one-dimensional 10-ring zeolite. The 10-ring channels in EU-1 zeolite have very large 12-ring pore extensions (12-ring side pocket), illustrated in Figure 1.10. The 10-ring channels in EU-1 zeolite have dimensions 5.4 × 4.1 Å [12], and the 12-ring side pockets are 6.8 × 5.8 × 8.1 Å [38]. The maximum diameter of a sphere that can be included in the channels of EU-1 is 7.00 Å [9].

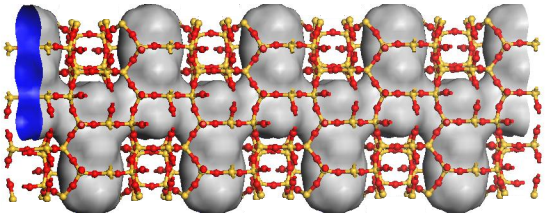

Figure 1.10: Illustration of the channel systems of EU-1 zeolite

SZR (SUZ-4): SUZ-4 zeolite has a three-dimensional channel system made from small (8-rings) and medium (10-rings) pore, illustrated in Figure 1.11. The 10-ring channels run in one-dimension and the 8-ring channels are perpendicular to it. The 10-rings are 4.1 × 5.2 Å in size, and the 8-rings have dimensions 4.8 × 3.2 Å viewed along [010] and 4.8 × 3.0 viewed along [110]. The maximum diameter of a sphere that can be included in the channels of SUZ-4 is 6.27 Å [9].

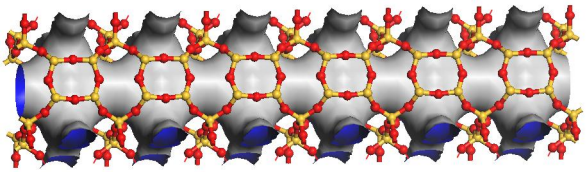

Figure 1.11: Illustration of the channel systems of SUZ-4 zeolite

CHA (SAPO-34): SAPO-34 is a three-dimensional small pore Zeotype material, constructed from Si, Al, and P T-atoms. The pore system in SAPO-34 catalyst consists of large cages that are connected with 8-ring windows of 3.8 × 3.8 Å dimensions. The maximum diameter of a sphere that can be included in the cages of SAPO-34 is 7.37 Å [9].

MFI (ZSM-5): ZSM-5 is a three-dimensional medium pore zeolite made from interconnecting straight and sinusoidal 10-ring channels. The straight and sinusoidal channels have dimensions 5.3 × 5.5 Å and 5.4 × 5.6 Å respectively. The maximum diameter of a sphere that can be included in the channels of ZSM-5 is 6.36 Å [9].

***BEA (Beta):** Beta is a disordered three-dimensional large pore zeolite consisting of 12-ring pores of dimensions 7.3 × 7.1 Å and 5.6 × 5.6 Å. The maximum diameter of a sphere that can be included in the channels of Beta is 6.68 Å [9].

2. Methanol to Hydrocarbons (MTH)

The global demand for energy and petrochemical products has been increasing over the years and it is forecasted that crude oil reservoirs will continue to deplete. This calls for both alternative and supplementary sources to supply the planet with fuel and chemicals in the future. Alternative carbon sources such as coal, natural gas, petrochemical residue, agricultural wastes, municipal garbage, wood etc are believed to be successors of the depleting crude oil in the future [35]. Even CO_2 is considered to be the future carbon source [39, 40]. Methanol is a highly relevant chemical intermediate in this respect, because it may be produced from practically any of the carbon sources mentioned above. The conversions of methanol to hydrocarbons (MTH) constitute the final step in the conversion of such alternative sources to value added products. The MTH reaction is presented in this chapter. An overview of the historical development of the process (section 2.1) and MTH reaction mechanisms (section 2.2) are provided. The contribution of this Ph.D. work towards further understanding of the MTH reaction is presented in section 4.2 and in the appropriate papers.

2.1. Historical development

The catalytic conversion of methanol to hydrocarbons (MTH) was fortuitously discovered by Mobil in the 1980s, following the first and the second oil crises in 1973 and 1979 [41]. Researchers at Mobil were trying to discover new ways of making high octane gasoline from methanol and isobutane over ZSM-5 [42, 43]. They imagined that methanol would be added to isobutane to form highly branched higher alkanes. Instead, a wide range of hydrocarbons were formed from methanol even when the isobutane feed was cut. Shortly after the discovery, effects on the development of the process have led to bench-scale and pilot-scale demonstration plants. Since then the MTH chemistry has been studied for decades over several zeolite and Zeotype materials. Depending on the catalyst topology and process conditions used, a wide range of product distribution could be obtained during the MTH reaction [44]. Commercial or near-commercial processes such as methanol to olefins (MTO); methanol to gasoline (MTG); and methanol to propene (MTP) are developed [36].

- *The methanol to gasoline (MTG) process* is catalyzed using the medium pore zeolite, ZSM-5. In this process methanol is converted to mainly gasoline range hydrocarbons (C_5+). The first MTG plant was built and commercialized in New Zealand by Mobil in

1985, with a production of 14500 barrels per day (about 30% of the country's need) of gasoline. Later as oil prices decreased the MTG section of the unit was shut down, and only the methanol production part from natural gas is in operation [45-47].

- *The methanol to olefins (MTO) process* is catalyzed using small pore Zeotype material, SAPO-34. In this process methanol is converted to light alkenes, mainly ethene and propene. The narrow pores of the material restrict diffusion of large hydrocarbons. The MTO technology has been demonstrated in a demo plant by Norsk Hydro [48].
- *The methanol to propene (MTP) process* is catalyzed using ZSM-5 catalyst. In this case, methanol is converted to propene with some by-product gasoline and LPG type fuels. The selectivity of the process is optimized towards propene by high temperature and low pressure employed during the reaction, as well as recycling of the heavier hydrocarbons. The process is developed by Lurgi [49].

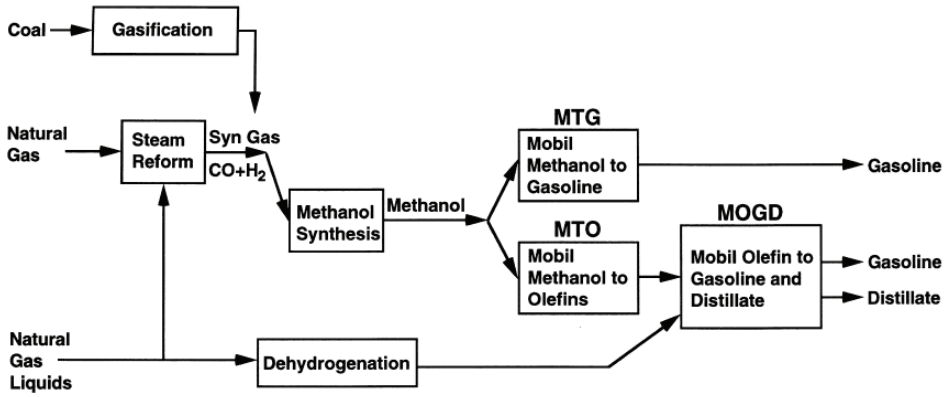

Figure 2.1: Gasoline and distillate production via methanol and Mobil's ZSM-5 technology. Adapted from Refs. [36, 50]

Figure 2.1 illustrates Mobil's MTG production through upgrading of coal, natural gas and oil. Light olefins produced during gasoline production are further converted to higher hydrocarbons through another ZSM-5 based process: Mobil's olefin-gasoline and distillate process (MOGD). In the MOGD reaction, ZSM-5 oligomerises light olefins into higher-molecular-weight olefins that fall into the gasoline, distillate and lubricant range [36, 50].

Following the Mobil's MTG technology, several other technologies for production of gasoline and light hydrocarbons were developed. Table 2.1 presents an overview of the industrial scale process developments and new licensing agreements of the MTH reaction.

Table 2.1. An overview of the MTH process development

Year	Developed by	Process	Statues
1981-1984	Mobil	MTG	Demonstrated on a 4 b/d plant in Paulsboro, NJ, USA
1981-1984	Mobil	MTG	Demonstrated on a 100 b/d plant in Wesseling, Germany.
1985	Mobil	MTG	Commercialized in New Zealnad (14500 b/d).
1980s	Haldor Topsøe	TIGAS[b]	A demonstration plant developed based on ZSM-5 (1 t/d) [51].
2008	UOP	MTO	UOP agreed with Viva Methanol Limited, a subsidiary of EuroChem. A commercial-scale plant is expected to come on stream in 2012 in Nigeria [52].
2009	Shanxi Coal Institute	MTG	A demonstration plant brought on stream in Shanxi, province, China (100 kt/y) [53].
2010	CAC Chemnisz	STF	Currently in a demonstration phase syngas-to-fuel unit, developed in Germany.
2010	Shanxi Coal Institute	MTG	Currently in a demonstration phase, developed in Chain.
2010	Haldor Topsøe	TIGAS	Currently being demonstrated in Des Plaines, USA, where a wood gasifier is running.
2009	UOP/INEOS and Total OCP[a]	MTO	A semi-commercial demonstration unit built in Feluy, Belgium (10 t/d).
2011	UOP/INE OS and Total OCP	MTO	Construction of a plant in Nanjing, China announced (295 kt/y) [53].
2010	Dalian Institute for Chemical Physics	DMTO[c]	A plant based on SAPO-34 started in Baotou, China (600 kt/y) [53].
2010	Lurgi	MTP	First plant started in China (500 kt/y propene and 185 kt/y gasoline) [53].
2012	ExxonMobil	MTG	Announced a licensing agreement with Sundrop Fuels Inc. (3, 500 b/d) [54].
2012	UOP	MTO	Announced a licensing agreement with China's Jiutai Energy (Zhungeer) Co. Ltd. [55].

[a]Olefin cracking process, [b]Topsøe integrated gasoline synthesis process, [c]Dalian methanol to olefins

As seen from Table 2.1, in the last four years there has been an increased interest in the industrial commercialization of the MTH process. This illustrates the vital importance of the process at the current time as well as in the near future.

2.2. Reaction mechanism

Since the discovery of the MTH reaction by Mobil, researchers have been working on reaction mechanism investigations. The early MTH mechanistic works were devoted to formation of direct carbon-carbon bonds from C_1 units (methanol or dimethyl ether), and several mechanisms were proposed [53]. However, high energy barriers are involved in the

direct coupling of C_1 units, and the mechanisms lack experimental evidences [53]. Song et al. performed the MTH reaction using extremely purified reagents and reported an increased induction period (a decreased initial rate of methanol conversion) [56]. It was suggested from the observation that the rate at which the direct coupling operates is irrelevant compared to the rate at which trace impurities initiate the reaction. Now the MTH reaction is believed to proceed through an indirect mechanism, wherein hydrocarbon species act as reaction centers for product formation [53, 57-59]. The hydrocarbons that act as reaction centers may be alkenes [60, 61], aromatic species [62-67], or both alkenes and aromatics simultaneously [62]. In the following section, the mechanisms involving hydrocarbons as reaction centers are presented. The ideas behind these reaction mechanisms root back to the early-1980s or earlier, and they are not presented in a chronological order.

Alkene based mechanism

Dessau and co-workers from Mobil proposed the alkene methylation/cracking mechanism for the MTH reaction in 1982, illustrated in Scheme 2.1 [60, 61].

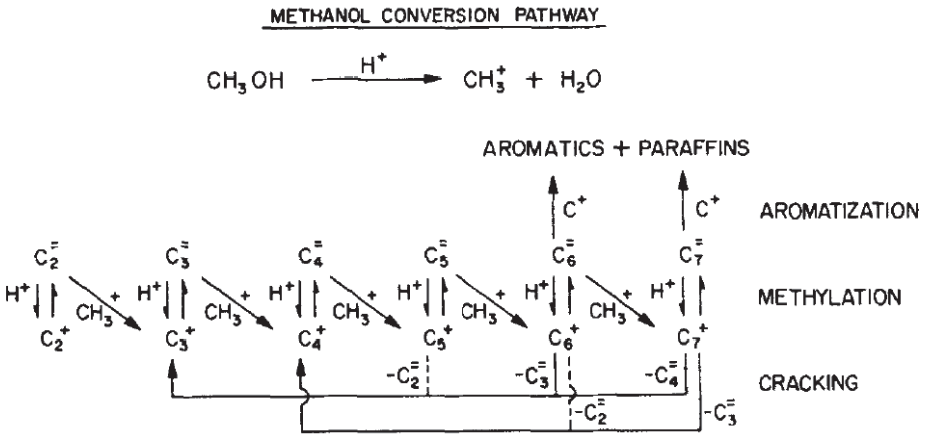

Scheme 2.1: Methylation/cracking mechanism proposed by Dessau. Adapted from Refs. [60, 61]

According to Dessuau's proposal methanol is believed to be converted to hydrocarbons through repeated methylation of light alkenes to form higher alkenes which in turn undergoes further methylation or cracking reactions. According to this mechanism, the initial alkenes are formed from reactions involving carbon-carbon bond formation, once alkenes are formed, the reaction leading to the their formation is irrelevant. In a similar proposal in 1986, Dessau stated that asking where the first olefin molecule comes from is analogous to asking where the

first peroxide comes from in autooxidation reaction. The statement further illustrates that the first olefins are important only during the initiation phase of the reaction, which is responsible for producing little of the total product observed. The first olefin could also come from impurities in the zeolite, reactant methanol or carrier gas. As little as a single olefin molecule was speculated to be enough to trigger the MTH reaction. Dessau's MTH reaction mechanism considers ethene as a product obtained from secondary re-equilibration of primary olefins and not as a primary product obtained from methanol. In addition, aromatic species formed during the MTH reaction are only presented as end products resulting from hydrogen transfer reactions, and does not explain their contribution to product formation.

Aromatic based (hydrocarbon pool) cycle

An alternative indirect mechanism is based on aromatics as reaction centers. In 1983 Mole and co-workers studied the MTH reaction over ZSM-5 catalyst and reported that addition of small amounts of toluene or p-xylene accelerates the MTH reaction [68, 69]. The result was ascribed to the alkylation of methyl group on the aromatic ring leading to olefin elimination, and the effect was called aromatic co-catalysis. The observation by Mole and co-workers was in agreement with Langner's report in 1982, in which the importance of cyclic compounds in the reaction pathway from methanol to hydrocarbons was highlighted [70]. Later, in the mid-1990's, Dahl and Kolboe proposed the "hydrocarbon pool mechanism" for the MTH reaction [57, 59]. They carried out isotopic labeling experiments by co-feeding olefin precursors (ethanol, propanol) and ^{13}C-methanol over a SAPO-34 catalyst. Analysis of the effluent showed that the alkenes were inert and most of the products were formed exclusively from methanol under the applied reaction condition [57-59]. Hence, a parallel indirect mechanism the "hydrocarbon pool" was proposed, illustrated in Scheme 2.2.

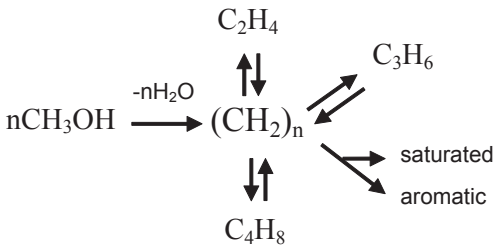

Scheme 2.2: The hydrocarbon pool mechanism as proposed by Dahl and Kolboe. Adapted from Refs. [57-59].

According to the hydrocarbon pool mechanism, species trapped in the zeolite/zeotype materials act as reaction centers for methanol conversion. The initial hydrocarbon pool was given an overall stoichiometry $(CH_2)_n$, and the chemical structure was not specified [57-59]. Detailed studies on the identity and activity of the hydrocarbon pool species have shown that polymethylbenzenes (methylated benzene molecules) act as the main reaction centers for the MTH reaction [62-67]. Unlike Dessau's mechanism, light alkene formation including ethene from the hydrocarbon pool species is well documented. In addition, Dessau's mechanism considers aromatic species as end products of the catalytic cycle, however, according to the hydrocarbon pool mechanism these species are actively involved in the reaction. The activity of the polymethylbenzene hydrocarbon pool species is also dependent on the catalyst topology. For example, for H-SAPO-34 and H-Beta catalysts higher polymethylbenzenes intermediates (penta and hexamethylbenzene) were shown to be more active than the lower methylbenzene intermediates (toluene-trimethylbenzene) [67, 71]. This is ascribed to the relatively large space found in the catalysts giving enough room for the higher polymethylbenzene intermediates [67, 71]. Contrary to this, for H-ZSM-5 zeolite the lower polymethylbenzenes were found to be more active intermediates than the higher polymethylbenzenes [67, 71] due to the steric limitation imposed by the relatively narrow pores of H-ZSM-5 catalyst. It is important to note that the alkenes formed from the hydrocarbon pool are controlled by the identity of the methylbenzene intermediate involved. For H-Beta higher methylbenzene intermediates favor the formation of propene and butenes [67], and for H-ZSM-5 catalyst lower methylbenzene intermediates favor the formation of mainly ethene and some of propene [71].

It is now generally accepted that polymethylbenzenes and other hydrocarbon pool species are reaction centers during methanol conversion over catalysts that provide enough space for the hydrocarbon pool mechanism. Two distinct possible pathways for alkene elimination of alkenes from hydrocarbon pool species have been proposed, illustrated in Scheme 2.3. The pathways are the side chain methylation and the paring routes.

Scheme 2.3 (side chain cycle) illustrates the side chain methylation route, which was proposed by Mole and co-workers [68, 69] and later refined by Haw and coworkers [72, 73]. According to this route, alkene elimination starts with the deprotonation of heptamethylbenzenium ion to HMMC (1,2,3,3,4,5-hexamethyl-6-methylene-cyclohexadiene). The exocyclic double bond on the HMMC is methylated to form an ethyl group, which is eliminated as ethene, or the ethyl group is further methylated to from an isopropyl group and it will detach form the ring as propene.

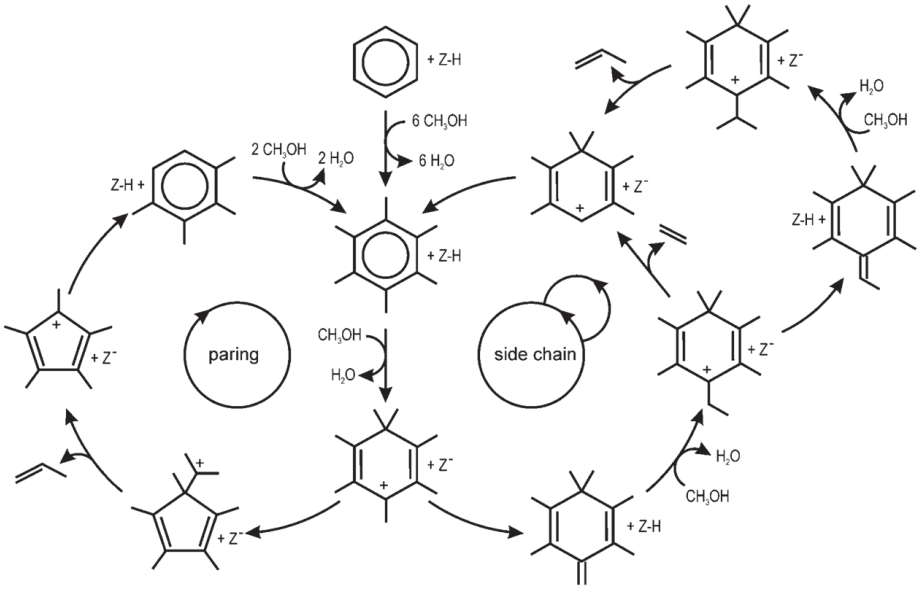

Scheme 2.3: The paring and side chain reaction routes for alkene elimination. Adapted from Ref. [74]

Alternatively, alkene elimination may follow the paring route, Scheme 2.3 (paring cycle). The complete cycle of the paring route involves contraction of aromatic ring to a 5-ring intermediate followed by expansion of the 5-ring back to 6-ring aromatics. This contraction and expansion of the ring leads to extension of the alkyl chain on the ring, and a carbon atom interchanges between the ring and the methyl-substituent. In this context, the word paring refers to an imagined process where methyl groups are shaved off the methylbenzene as alkenes. Experiments involving co-reaction of ^{12}C benzene and ^{13}C methanol revealed that alkene elimination in agreement with the paring route is favored over zeolite Beta [75] and SAPO-5 catalyst [76]. The paring route was adapted from a similar mechanism proposed by Sullivan et al. in 1961 to rationalize the product distribution observed when hexamethylbenzene was reacted over a bifunctional nickel sulfide on silica–alumina catalyst or over the purely acidic silica–alumina support [77].

Dual cycle concept

Recently, isotopic labeling experiments performed over ZSM-5 catalysts showed that ethene and lower methylbenzenes are mechanistically linked through an aromatic based hydrocarbon pool cycle but separated from the formation of higher alkenes [62, 66]. Higher alkenes (C_3+) displayed a different reactivity for the incoming methanol than the methylbenzenes and

ethene, suggesting an additional reaction mechanism working in parallel with the aromatic based hydrocarbon pool mechanism.

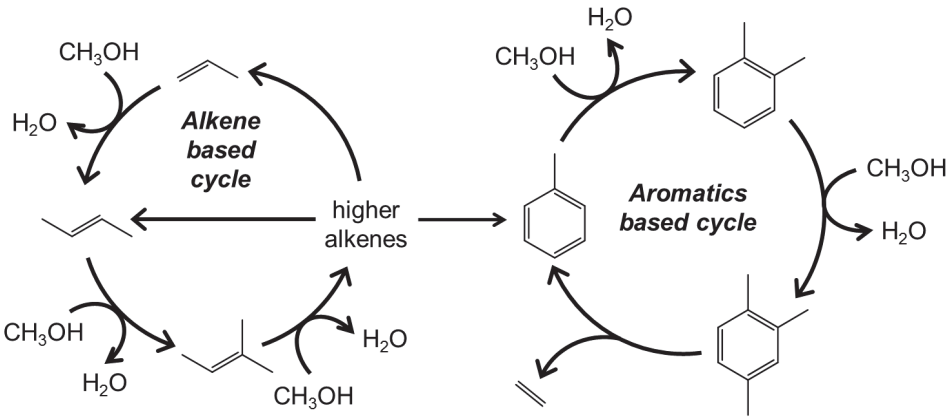

Scheme 2.4: Suggested dual cycle concept for methanol conversion. Adapted from Ref. [62]

The two mechanistic cycles running simultaneously during the methanol to hydrocarbons reaction over a ZSM-5 catalyst were described using the dual cycle concept, illustrated in Scheme 2.4 [62]. Accordingly, the aromatic based cycle is in agreement with the generally accepted hydrocarbon pool mechanism [57, 59], in which methylbenzene molecules are repeatedly methylated followed by alkene elimination in a later reaction step. On the other hand, the alkene based cycle is based on repeated alkene methylation and cracking steps according to the scheme originally proposed by Dessau [60, 61], yields mainly C_3+ alkenes, but only minor amounts of ethene. The dual cycle concept introduced an interesting question regarding whether one of the cycles can run independently and if it could be possible to manipulate the relative contribution from these cycles to the product formation, thereby controlling the selectivity. Further work on reaction mechanism investigations was performed in this Ph.D. work and the results are presented in section 4.2.

3. Experimental

The following chapter provides a general description of the experimental procedures and methods employed in this work. Descriptions of catalyst synthesis (section 3.1), characterization (section 3.2), catalytic tests (section 3.3), and isotopic labeling calculations (section 3.4) are provided.

3.1. Catalyst synthesis and preparation

Most of the zeolite catalysts employed in this thesis are in-house synthesized. The synthesis was carried out under hydrothermal conditions as outlined in section 1.2. Prior to the synthesis the Teflon liner and Teflon coated bar magnets were cleaned in 15% HF and rinsed with distilled water. Commercially available ZSM-22 (Si/Al = 50) and ZSM-23 (Si/Al = 23) supplied by Zeolyst International were also investigated.

Synthesis of ZSM-22

ZSM-22 was synthesized following the synthesis procedure in Ref. [78], with gel composition:

8.9 K_2O : Al_2O_3 : 90 SiO_2 : 3 K_2SO_4 : 27.3 DAO : 3588 H_2O.

- Aqueous solution of 2.39 g potassium hydroxide (Sigma-Aldrich, >85 %) in 10.89 g water, 1.06 g aluminum sulfate (J. T. Baker, >98 %) in 10.89 g water, and 6.23 g diaminooctane (Fluka, >98 %) in 43.6 g water were mixed.
- 28.5 g Ludox AS-30 solution (Aldrich, 30 wt%) in 16.14 g water was added to the solutions above under stirring.
- The gel was transferred into a 45 ml Teflon lined stainless steel autoclave, and crystallized in an oven with an inset that tumbles the autoclave (37 rpm) for 3 to 4 days at 160 °C. Teflon coated bar magnet was placed in the liner to enhance the gel mixing during crystallization.

A static synthesis using the above synthesis gel resulted in crystallization of a pure ZSM-11 zeolite, which is in agreement with the previous report [79]. Therefore, it is essential to have a good gel mixing during crystallization to avoid formation of ZSM-11 impurity. Furthermore,

a dense phase cristobalite was frequently observed; hence, a good control of crystallization time is required. Previous studies have also reported cristabolite as an impurity phase [80, 81].

Synthesis of EU-1

The synthesis of EU-1 was based on a combination of procedures reported by Shin et al. [82] and Lee et al. [83], from a gel with the following composition:

60 SiO_2 : Al_2O_3 : 18 Na_2O : 9 $HMBr_2$: 2670 H_2O

- Aqueous solutions of clear 0.36 g aluminum nitrate (Sigma-Aldrich, >98 %) in 18.02 g of water and 0.68 g sodium hydroxide (Merck, >99 %) in 0.68 g water were mixed and stirred until a homogeneous solution was obtained.
- 1.55 g hexamethonium bromide (J&K Chemica, 98 %) was added to the aqueous solution above and homogenized under stirring.
- At last, 5.71 g Ludox AS-30 (Aldrich, 30 wt%) was added and manually stirred for five minutes.
- The gel was transferred into a 45 ml Teflon lined stainless steel autoclave and crystallized in an oven with an inset that tumbles the autoclave (37 rpm) for 14 days at 160 °C. Teflon coated bar magnet was placed in the liner to enhance the gel mixing during crystallization.

Synthesis of ZSM-48

ZSM-48 was synthesized using pre-prepared pentamethonium bromide ($PMBr_2$) as a structure directing agent (SDA), as described in the literature [83]. Briefly, 15 g dibromopentane (DBP) (Aldrich, 97 %) was mixed with 31.1 g trimetylamine (TMA) (Aldrich, 33 wt%) solution in ethanol (Sigma-Aldrich, 99.8 %) and additionally 75 ml ethanol, giving a relative molar ratio of 2.5:1 of TMA:DBP. The mixture was refluxed over night, cooled down, filtered and dried at 70 °C. ZSM-48 was synthesized from a gel with the following composition:

80 SiO_2 : Al_2O_3 : 13.3 Na_2O : 12 $HMBr_2$: 3200 H_2O

- Aqueous solutions of 0.22 g aluminum nitrate (Sigma-Aldrich, >98 %) in 17.93 g water and 0.32 g sodium hydroxide (Merck, >99 %) in 0.32 g water were mixed and stirred until a homogeneous solution was obtained.

- To the resulting solution, 1.24 g of the SDA was added and stirred until a homogenous solution was obtained.
- At last 4.96 g tetraethyl orthosilicate (TEOS) (Sigma-Aldrich, 98 %) was added and stirred until all the ethanol was evaporated.
- The final gel was transferred into a 45 ml Teflon lined stainless steel autoclaves and the crystallization was performed in an oven with an inset that tumbles the autoclaves (37 rpm) at 160 °C for 7 days. Teflon coated bar magnet was placed in the liner to enhance the gel mixing during crystallization.

Lee et al. [83] has investigated the effect of using diquaternary alkylammonium ions ($(CH_3)_3N^+(CH_2)_nN^+(CH_3)_3$) as a template for the synthesis of ZSM-48 zeolite. Pure ZSM-48 can be synthesized using templates of this class where n = 3, 5, 6, 8, 9 or 10 without Al in the syntheses gel (Si/Al = ∞). However when Al is added in the gel (Si/Al = 60), ZSM-48 is obtained only when n = 3, 5 and 10. When the amount of Al is further increased in the gel (Si/Al = 30), only n = 5 gives ZSM-48. In this work, several syntheses were performed using hexamethonium bromide (n = 6) [84] and using tetramethylammonium [85] as template, however, incorporation of Al in the framework of ZSM-48 was not successful. Therefore, it is important to use pentamethonium bromide (n = 5) as a template for obtaining acidic ZSM-48.

Synthesis of SUZ-4

SUZ-4 was synthesized following the synthesis procedure in Ref. [86], with gel composition:

7.92 K_2O : Al_2O_3 : 16.21 SiO_2 : 1.83 TEAOH : 507 H_2O

- 0.4 g aluminum wire (Sigma-Aldrich, 99 %) was dissolved in 3.3 g potassium hydroxide solution (Sigma-Aldrich, >85 %) in 50.6 g water.
- 7.93 g tetraethylammonium hydroxide (TEAOH) (Sigma-Aldrich, 25 wt%) and 18.23 g LUDOX AS-40 (Sigma-Aldrich, 40 wt%) were added successively to the Al solution.
- The resulting gel was transferred into a 45 ml Teflon lined stainless steel autoclaves and crystallized in an over with an inset that tumbles the autoclaves (37 rpm) at 160 °C for 3 to 7 days. Teflon coated bar magnet was placed in the liner to enhance the gel mixing during crystallization.

The above gel composition typically gives pure SUZ-4 in a wide temperature range (140-180 °C). Several attempts were made to crystallize SUZ-4 with less Al in the product, using different sources of Si and reduced amounts of Al. However, synthesis gel with lower amounts of Al resulted in a lower yield of the SUZ-4 product without changing the Si/Al. In addition, a number of attempts to crystallize SUZ-4 with different morphologies were made by changing the amount of water and source of Si. However, the material typically crystallizes with needle-like morphology. Both changing the Si/Al in the product and changing morphology attempts were not successful. However, in both cases pure SUZ-4 was obtained.

Calcination and ion-exchange

The organic templates were removed by calcination under a flow of pure oxygen, oxygen/nitrogen mixtures or static air at high temperatures. ZSM-48 and EU-1 zeolites were calcined in 50:50 N_2/O_2 mixtures for 9 hours, including 4 hours during which the temperature increased from ambient to 500 °C. ZSM-22 and ZSM-23 were calcined under a flow of pure oxygen at 550 °C for 12 hours. SUZ-4 zeolite was calcined in static air at 550 °C for 6 hours. The calcined samples were ion exchanged 3 × 2 hours with 1M NH_4NO_3 (Fluka, >99 %) in a 70 °C water bath. The protonated zeolite with Brønsted acidity is obtained after desorption of ammonia at 550 °C.

3.1. Catalyst characterization

In order to obtain physical and chemical information about the zeolite catalysts, a number of characterization methods were employed. Powder X-ray diffraction (XRD), Scanning Electron Microscopy (SEM), Transmission Electron Microscopy (TEM), Ammonia-Temperature Programmed Desorption (NH_3-TPD), Aluminum Nuclear Magnetic Resonance (^{27}Al-NMR), N_2-Sorption Measurements, Fourier Transform Infrared Spectroscopy (FTIR) and Thermogravimetric Analysis (TGA) were used. The experimental conditions are outlined below.

Powder XRD

The phase purity and crystallinity were identified using X-ray diffraction on a Siemens D-5000 diffractometer with Bragg-Scherrer geometry, position sensitive detector and CuK_α

radiation (λ= 1.5406 Å). XRD data were analyzed using EVA 8.0, developed by SOCABIM. The diffraction pattern was compared with the data in the powder diffraction file (PDF) database compiled and revised by Joint Committee on Powder Diffraction Standards International Centre. Furthermore, Pawley fitting analyses using standard structures as implemented in Materials Studio 5.0 software were performed.

SEM

Scanning Electron Microscopy (SEM) was used for crystal size/shape and purity determination. The zeolite crystals were sprinkled on a carbon tape mounted on aluminum stub. Energy-Dispersive X-ray (EDS) analyses were performed to investigate the elemental composition. The analysis was performed on a Quanta 200 F (FEI).

TEM

Transmission Electron Microscopy (TEM) analyses were performed on Philips C200, at Haldor Topsøe A/S, Denmark. Gold was used as internal diffraction standard to obtain exact lattice spacings.

N_2-sorption measurements

The surface area of the catalysts was determined using the BET method by nitrogen adsorption in a range of relative pressure 0 - 0.99 P/P_o at 77 K. About 60 mg of the catalysts were outgassed for 5 hours (1 hour at 80 °C and 4 hours at 300 °C) prior to the surface area measurements. The measurements were performed using a BELSORP-mini II instrument.

^{27}Al-NMR

The samples were packed in a zirconium rotor, 4 mm diameter, and a Kel-F cap. Al-NMR spectra were recorded using a Bruker AMX-200 instrument. A frequency of 52.138 MHz, and spinning speed of 5 kHz was used. A number of 64k (i.e. 65536) scans were accumulated with a recycle delay of 10 ms.

NH_3-TPD

150-300 mg of zeolite powder activated at 500 °C under the flow of nitrogen for 1 hour (75 ml/min). The samples were cooled to and kept at 150 °C for 30 minutes, under the flow of 2% NH_3 in helium (75 ml/min). Physisorbed ammonia was removed by flushing the sample with

nitrogen at 150 °C for 2 hours (75 ml/min). At last, the temperature of the oven was increased to 740 °C with heating ramp 10 °C/min under the flow of nitrogen (75 ml/min), and the desorbed ammonia was detected using an on-line mass spectrometry (MS). The acid site density of the materials is calculated assuming adsorption of one ammonia molecule per acid site. The NH_3-TPD experiments were performed at Holder Topsøe, Denmark.

FTIR

FTIR is a commonly used technique for investigating acid sites in protonated zeolites. Typically, the interaction of the active site in the zeolite framework with a probe molecule such as carbon monoxide (CO) or pyridine is recorded. The interaction of zeolite active sites with the probe molecule will result in changes in the absorption of energy in the infra red region of the spectrum, from which the type and strength of the active site is determined. Details on the investigation of zeolites using FTIR can be found in literature [87, 88].

In this thesis, thin self-supporting wafers were prepared and their transmittance for IR radiation was checked prier to pretreatment. The wafers were pretreated under vacuum for 3 hours. 1 hour at temperatures 120, 350, and 450 °C. Spectra were collected on FTIR Bruker vertex 80 with MCT detector, working at 2 cm^{-1} resolution and a number of 64 scans. CO was used as a probe molecule, and its interaction with the catalysts was followed at a temperature of 77 K by using liquid nitrogen as a coolant.

TGA

~10 mg of the catalysts (as-made or after reaction) was used for the experiments. The organic template or coke was removed by burning in oxygen. The temperature of the TGA instrument (Rheometric Scientific SAT 1500) was programmed between 25 and 600 °C (heating rate = 5 °C min^{-1}, hold time = 3 hours at 650 °C)

3.2. Catalytic tests

Most of the experiments in this thesis involve only methanol as a reactant, and these experiments were performed using a reactor system (test rig 1), described below. A few experiments involving the co-conversion of methanol and other alkenes is also studied using a different reactor system (test rig 2). The main difference between test rig 1 and test rig 2 is

that the effluent products are analyzed with online GC having different columns (outlined below). Therefore, schematic illustration of only one of the reactor systems (test rig 1) is provided.

The reactor system: Majority of the catalytic test experiments in this thesis were performed using a reactor system (test rig 1) originally designed by Rønning [89], illustrated in Figure 3.1. The reactor system is equipped with four gas supply lines: Line 1 to 4. Line 1, 2 and 3 are connected to helium and Line 4 is connected to oxygen. Lines 1 and 2 were fitted with saturation evaporators allowing the feeding of liquid reactants. Depending on the experiment, the saturation evaporators were filled with ^{12}C methanol, ^{13}C methanol or other alcohols. The flow of gases was regulated by Porter P-150 ball flowmeters and measured using ADM2000 Universal gas flowmeter, Agilent technologies. Desired reactant flow rates (WHSV) were achieved by adjusting the carrier gas flow and/or adjusting the temperature of methanol saturation water bath (0 or 20 °C). The temperature of the oven was monitored using a thermocouple fixed inside in oven.

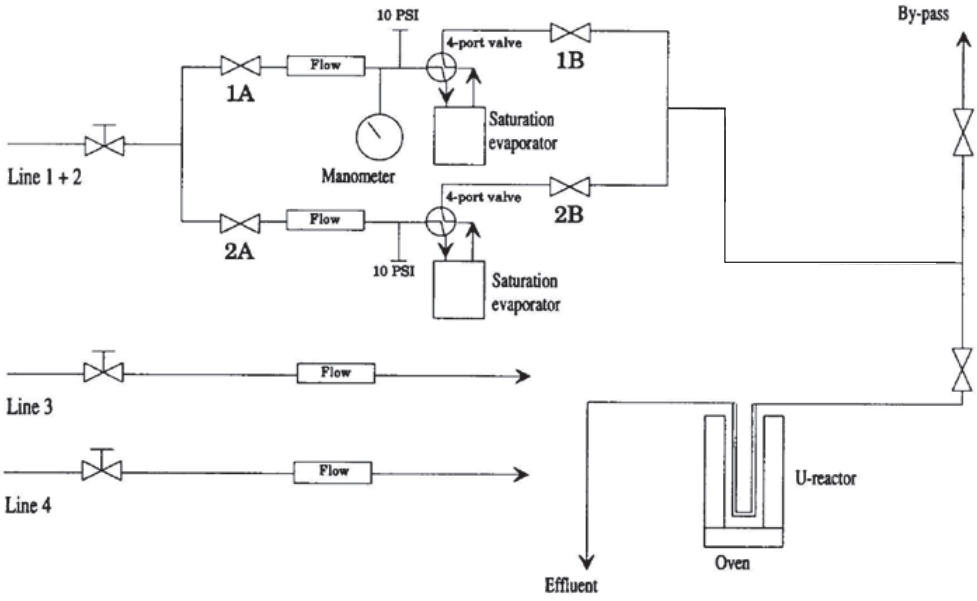

Figure 3.1: Schematic drawing of the reactor system

Catalytic test experiments: The catalytic test experiments were performed using fixed bed glass reactors with internal diameter 6 or 10 mm. The catalysts were pressed, gently crushed and sieved to particle sizes between 250 and 420 μm. The temperature of the reaction was

controlled using a thermocouple inserted in the reactor, at the bottom of the catalyst bed. Most of the experiments were carried out using 50 mg of catalyst. Before each test, the reactor was heated to 550 °C under a flow of helium. The catalysts were calcined *in situ* at this temperature with a flow of pure oxygen for 1 hour. The *in situ* calcination is performed to remove species adsorbed during catalyst handling and storage and is important for the reproducibility of the results.

Reaction product analyses: The MTH reaction gas phase effluent were analyzed using an online GC and offline GC-MS. Retained hydrocarbons within the zeolite pore during reaction were extracted and analyzed using offline GC-MS (see below).

- For the catalytic tests performed using test rig 1, an online gas chromatography connected to the outlet of the reactor using a heated transfer line was used to analyze the gas phase reactor effluent. An Agilent 6890 A GC with FID using a Supelco SPB-5 capillary column (60 m, 0.530 mm i.d., stationary phase thickness 3 μm) was used for the analysis. The temperature was programmed between 45 and 260 °C with a heating rate of 25 °C min^{-1} (hold time = 5 min at 45 °C and 16 min at the final temperature).
- For the reactions involving the co-conversion of methanol with other alkenes (test rig 2), the reactor outlet was connected to an Aligent 6890 GC equipped with a HP-PLOT Q column with FID detector. The temperature was programmed between 90 and 270 °C with a heating rate of 20 °C min^{-1} (hold time = 5 min at 90 °C, 5 min at 220 °C and 9 min at 270 °C).
- An offline GC-MS was used for analyzing the isotopic composition of the gas phase effluent (section 3.4). HP 6890 gas chromatograph equipped with a GS-GASPRO column (60 m, 0.32 mm) and a HP-5973 mass selective detector. The temperature was programmed between 100 and 250 °C with a heating rate of 10 °C min^{-1} (hold time = 10 min at 100 °C and 15 min at 250 °C). The compounds were identified by comparing with the mass spectral library of the NIST98 database.
- An offline GC-MS was used for analyzing organic species trapped in the channels of the catalysts during the MTH reaction after different times on stream. The analyses were performed by dissolving 20 mg of the used catalyst in a screw-cap Teflon vial using 1 ml 15% HF (Fluka, 40 %). The librated organics were extracted using 1 ml Dichloromethane (Merch, >99.9 %), with hexachloroethane (Supelco, 99.9 %) as internal standard, and analyzed using GC-MS. An Agilent 6890N gas chromatograph connected to an Agilent

5793 mass selective detector equipped with a HP-5MS column (60 m, 0.25 mm i.d., stationary phase thickness 0.25 μm) was used for the analysis. The temperature of the oven was programmed between 50 and 300 °C with a heating rate of 10 °C min per minute (hold time = 3 min at 50 °C and 15 min at 300 °C). The compounds were identified by comparing with the mass spectral library of the NIST98 database.

Calculation of conversion, selectivity and yield: Methanol conversion (X), product selectivity (S) and product yield (Y) were calculated based on GC-FID areas. During the calculations, methanol and dimethyl ether (DME), which is the condensation product of methanol molecules are considered as reactants, and all non-oxygen containing effluent hydrocarbons were considered as reaction products. The calculations were performed as follows:

For reactions involving only methanol in the reactant feed:

Conversion $$X_i(\%) = \frac{C\ in\ products - C\ in\ reactants}{C\ in\ all\ compounds} \cdot 100 \qquad (3.1)$$

Selectivity $$S_i(\%) = \frac{C_i}{C\ in\ all\ compounds} \cdot 100 \qquad (3.2)$$

Yield $$Y_i(\%) = \frac{X_i \cdot S_i}{100} \qquad (3.3)$$

For the reaction involving co-conversion of methanol with other alkenes, the product molecules cannot be used for the calculation of conversion due to the presence of the alkenes in both reactant and product streams. Hence, the calculation was based on only oxygen containing hydrocarbons. Area of oxygenates (methanol + DME) over fully deactivated catalyst was used as a reference area (C_{ref}). The conversion is calculated as follows:

Conversion $$X_i(\%) = 100 - \frac{C\ in\ reactants}{C_{ref}} \cdot 100 \qquad (3.4)$$

Selectivity and yield calculations were not performed for the co-conversion experiments. Instead, the effluent hydrocarbons are reported as reactor outlet composition. This is again due to complications caused by the presence of alkenes in both reactant and product streams.

3.3. Isotope labeling studies

Isotopic labeling is a commonly used method for elucidating MTH reaction mechanisms and identifying reactive species over zeolites [53]. In this thesis, two different experimental procedures were followed for identifying reactive species.

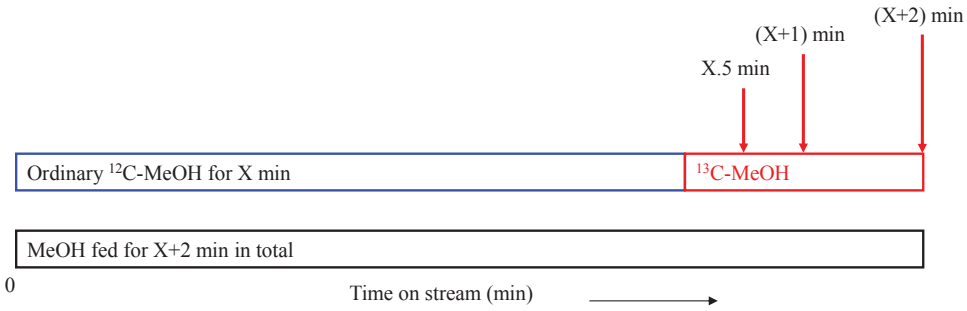

Figure 3.2: Illustration of isotopic switching experiment from a predefined time of ^{12}C methanol reaction to ^{13}C methanol.

The first procedure involves isotope switching to ^{13}C methanol over a working catalyst after a predefined time (X minutes) of reaction using ^{12}C methanol, illustrated in Figure 3.2. During such isotope switching experiments, reactive species in a working catalyst will display rapid incorporation and high amounts of total ^{13}C atoms within seconds or a few minutes. While, less reactive species will display a lower total ^{13}C atoms. In this thesis, experiments involving ^{12}C methanol reaction for 2, 5, 18 minutes or more followed by switching to ^{13}C methanol were performed. The incorporation of ^{13}C is investigated in the gas phase species and retained hydrocarbons inside the zeolite pores. For the gas phase effluent analysis samples were taken using a needle and syringe at the reactor outlet, and hydrocarbons retained inside the zeolite pores the reaction was quenched to room temperature, and the organics were extracted and analyzed as described in section 3.2.

The second procedure involves co-reaction of ^{13}C methanol and ^{12}C alkenes (formed *in situ* from alcohols). In this case, reactivity of the co-reactant alkene molecules with ^{13}C methanol is investigated from the isotopic composition of the products. The experiments were performed using ^{12}C methanol (BDH Laboratory Supplies, > 99.8 %) and ^{13}C methanol

(ICON, 99 %).. For the co-conversion reaction with methanol, other higher alcohols were added in the reactant stream as sources of alkene. Ethanol (Sigma-Aldrich, >99.8 %), isopropanol (Sigma-Aldrich, >99.8 %) and tert-butanol (Fluka, >99 %) were used as sources of ethene, propene and butene respectively.

Isotopic composition analysis

The isotopic composition analysis method used in this thesis was developed by Rønning [89]. Single ion chromatograms were extracted from total ion chromatograms (GC-MS), and the isotopic compositions were calculated. Two considerations were made:

i) *No kinetic isotope effects:* the mass spectrum of a specific compound is assumed to be independent of the number of ^{12}C and ^{13}C atoms in the molecule.
ii) Only molecular ions and fragment ions with intact carbon skeletons are analyzed. Therefore, for a given compound the variation in ionic masses will be a function of the number of hydrogen atoms and ^{13}C atoms in the ion.

Calculation of standard ^{12}C spectra

The isotopic composition calculation requires pure ^{12}C standard spectra of the compounds. Hence, correction for the natural abundances ^{13}C (1.11 %) is required. For an ion with N carbon atoms, the statistical probability that the ion contains n ^{13}C-atom is:

$$P_n = \frac{N!}{n!\,(N-n)!} \cdot 0.0111^n \cdot 0{,}9889^{N-n} \tag{3.5}$$

The corrected single ion peak area, $A_{corr}(i)$, for an ion with mass number *i,* is then given by:

$$A_{corr}(i) = A_{obs}(i) + \sum_{n=1}^{N} A_{corr}(i)P_n - \sum_{n=1}^{N} A_{corr}(i-n)P_n \tag{3.6}$$

Where $A_{obs}(i)$: Observed single ion peak area with ion mass *i* and n: number of ^{13}C atoms to be corrected for. Rearranging Equation 3.6 gives

$$A_{corr}(i)\left(1 - \sum_{n=1}^{N} P_n\right) = A_{obs}(i) - \sum_{n=1}^{N} A_{corr}(i-n)P_n \,, where \left(1 - \sum_{n=1}^{N} P_n\right) = P_0 = 0.9889^N \tag{3.7}$$

Where P_0: is the probability of the ion consisting exclusively of ^{12}C atoms. The expression for the corrected single ion peak area then reduces to:

$$A_{corr}(i) = \frac{A_{obs}(i) - \sum_{n=1}^{N} A_{corr}(i-n) \cdot P_n}{0.9889^N} \quad (3.8)$$

Where P_n: Statistical probability, A_{corr}(i-n): Corrected single ion peak area with ion mass i-n, and other symbols as before.

Calculation of isotopic composition

For calculating isotopic composition, single ion chromatograms extracted from the total ion chromatogram and integrated. The single ion peak area contains contributions from ions with the same mass numbers but with different number of hydrogen and ^{13}C atoms. For example, the area of the ion peak m/z = 36 for propene is from ^{12}C-^{12}C-^{12}C, m/z = 37 is contributions from ^{12}C-^{12}C-^{12}CH and ^{13}C-^{12}C-^{12}C, m/z = 38 is contributions from ^{12}CH-^{12}CH-^{12}C, ^{13}C-^{12}C-^{12}CH, and ^{13}C-^{13}C-^{12}C and so on. Based on such relations, the observed single ion peak area can be expressed as a linear combination of the fraction of ^{13}C atoms in the ion. Hence, every single ion peak area for an ion with mass number *i* can be expressed using a set of linear equations and solved using multivariable linear regression procedure. The calculation in solving regression problems can be expressed compactly using matrix notation, illustrated for propene below.

$$\begin{bmatrix} I_{36} \\ I_{37} \\ I_{38} \\ I_{39} \\ I_{40} \\ I_{41} \\ I_{42} \\ I_{43} \\ I_{44} \\ I_{45} \end{bmatrix} = a_0 \times \begin{bmatrix} S_{36} \\ S_{37} \\ S_{38} \\ S_{39} \\ S_{40} \\ S_{41} \\ S_{42} \\ 0 \\ 0 \\ 0 \end{bmatrix} + a_1 \times \begin{bmatrix} 0 \\ S_{36} \\ S_{37} \\ S_{38} \\ S_{39} \\ S_{40} \\ S_{41} \\ S_{42} \\ 0 \\ 0 \end{bmatrix} + a_2 \times \begin{bmatrix} 0 \\ 0 \\ S_{36} \\ S_{37} \\ S_{38} \\ S_{39} \\ S_{40} \\ S_{41} \\ S_{42} \\ 0 \end{bmatrix} + a_3 \times \begin{bmatrix} 0 \\ 0 \\ 0 \\ S_{36} \\ S_{37} \\ S_{38} \\ S_{39} \\ S_{40} \\ S_{41} \\ S_{42} \end{bmatrix}$$

$$observed \qquad 0\ ^{13}C \qquad 1\ ^{13}C \qquad 2\ ^{13}C \qquad 3\ ^{13}C$$

From the pattern in the matrix notation above, the observed area of an ion with m/z = 39 would then be given as

$$I_{39} = a_0 S_{39} + a_1 S_{38} + a_2 S_{37} + a_3 S_{36} \quad (3.9)$$

According to this equation, the observed single ion areas (*I*) are variables that can be expressed in terms of unknown regression coefficients a_0, a_1, a_2, and a_3 that provide fraction

of ions with 0 × ^{13}C, 1 × ^{13}C, 2 × ^{13}C and 3 × ^{13}C respectively. Note that, the isotope fractions shown in the matrix above (S_i) are normalized using the standard pure ^{12}C spectra of the compounds that are corrected for the natural abundance of ^{13}C. Recall that the goal of multivariable linear regression is to minimize the sum of the squared residuals. Regression coefficients that satisfy this criterion are found by solving the set of normal equations. An Excel spreadsheet programmed to formulate appropriate set of equations for a given compound and to solve the set of equations is used for the calculations.

The reliability of the calculated isotopic distribution is expressed by the correlation coefficient generated from the regression calculation. In addition, a root mean square parameter of the differences between the observed and calculated single ion peak areas is used. The root mean square is given by:

$$r.m.s = \sqrt{\sum \left(\frac{A_{obs}(i)}{A_{sum}(obs)} - \frac{A_{calc}(i)}{A_{sum}(calc)} \right)^2} \tag{3.10}$$

4. This work

4.1. Scope

The main objective of this Ph.D. thesis is to obtain new insight into the methanol to hydrocarbons reaction over one-dimensional 10-ring zeolites.

As mentioned in section 2.2, the MTH reaction is believed to proceed through indirect mechanisms, in which hydrocarbons within the catalyst pores act as reaction centers [53]. Studies have shown that both alkenes based and aromatic based reaction mechanisms operate simultaneously over ZSM-5 catalyst, highlighted using the dual cycle concept [66]. The authors introduced an interesting question regarding possibilities of controlling selectivity by tuning the relative contributions of the aromatic and alkene cycles, and if alkene based cycle can run more or less independently. Therefore it was decided to investigate the catalytic performance of one-dimensional 10-ring zeolites, thereby addressing the questions raised during the introduction of the ducal cycle concept.

We stated the investigation using ZSM-22 as a catalyst for the MTH reaction. Over time, the work was continued over other one-dimensional 10-ring zeolites, namely ZSM-23, EU-1 and ZSM-48 catalysts. The one-dimensional 10-ring zeolites included in this thesis have comparable 10-ring channels sizes, but they are different in channel shapes and pore extensions (side pockets). It was therefore decided to investigate the influence of subtle changes in zeolite pore size/shape on shape selectivity of zeolite catalysis. In addition, SUZ-4 zeolite that consists of 10-ring channels running in one-dimension and connected with 8-ring channels is investigated. SUZ-4 is included in the investigation assuming that the material is likely to behave as a one-dimensional 10-ring zeolite, since the diffusion of product molecules should be faster through the 10-rings.

This chapter presents the summary of the results of the Ph.D. work. A detailed discussion of the results is provided in the Appendix as published papers or articles in preparation.

4.2. Summary of results

Zeolites or Zeotype materials such as ZSM-5, SAPO-34 and Beta are extensively studied as catalysts for the methanol to hydrocarbons reaction [64, 65, 71, 75, 90-102]. ZSM-5 and SAPO-34 catalysts are studied due to the potential of industrial production of gasoline and olefins over the catalysts respectively. The studies over Beta are mainly for reaction mechanism investigations. One-dimensional 10-ring zeolites are less studied as catalysts for the methanol to hydrocarbons reaction. In this section, a summary of the MTH reaction over ZSM-22, ZSM-23, ZSM-48, EU-1 and SUZ-4 is presented. Emphasis is given to shape selectivity, rather than catalyst stability and characterization results. Shape selectivity of ZSM-22 during the MTH reaction (paper I) is presented first, and parameters that influence shape selectivity such as: reaction mechanism (paper II), pore size and shape (paper III), coke deposition (paper III), catalyst particle morphology (IV) are highlighted. A section on how to optimize the shape selectivity of ZSM-22 catalyst (paper V) is provided. Details on characterization results, test conditions, catalyst stability, and retained hydrocarbons are attached in the Appendix as published article or article in preparation.

Shape Selectivity in one-dimensional 10-ring zeolite ZSM-22: ZSM-22 catalyst was reported as inactive for methanol conversion due to the narrow pores of the material, which were believed to be insufficient to accommodate the space demanding hydrocarbon pool species [103-106]. However, in our work, we found that at suitable reaction conditions, ZSM-22 can convert methanol to hydrocarbons for several hours.

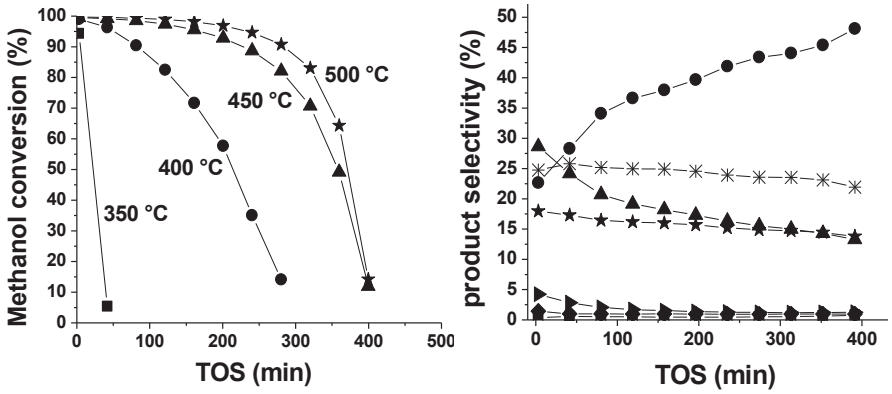

Figure 4.1: Methanol conversion as a function of time on stream at different temperatures (left panel), and selectivities towards C_1■, C_2►, C_3▲, C_4=★, C_4-◆, C_5✳ and C_6+● (right panel), at 400 °C and WHSV = 2 $gg^{-1}h^{-1}$.

Figure 4.1 displays methanol conversion at different temperatures (left panel) and selectivity towards various hydrocarbons at 400 °C (right panel) as a function of time on stream, and WHSV = 2 $gg^{-1}h^{-1}$. In contrast to previous reports, ZSM-22 found to be an active catalyst for methanol conversion. Temperature above 350 °C and low feed rates are required for appreciable methanol conversion. The work by Song and co-workers [105] over ZSM-22 showed a low production of olefins during the first pulses of methanol but the amount of olefin quickly decreased to essentially zero. The observed olefin production was ascribed to presence of ZSM-11 impurity. Similar conclusions were reached in a flow type experiments (not pulses) by Song et al. (WHSV = 48 $gg^{-1}h^{-1}$) [105] and Li et al. (WHSV = 10 $gg^{-1}h^{-1}$) [103].

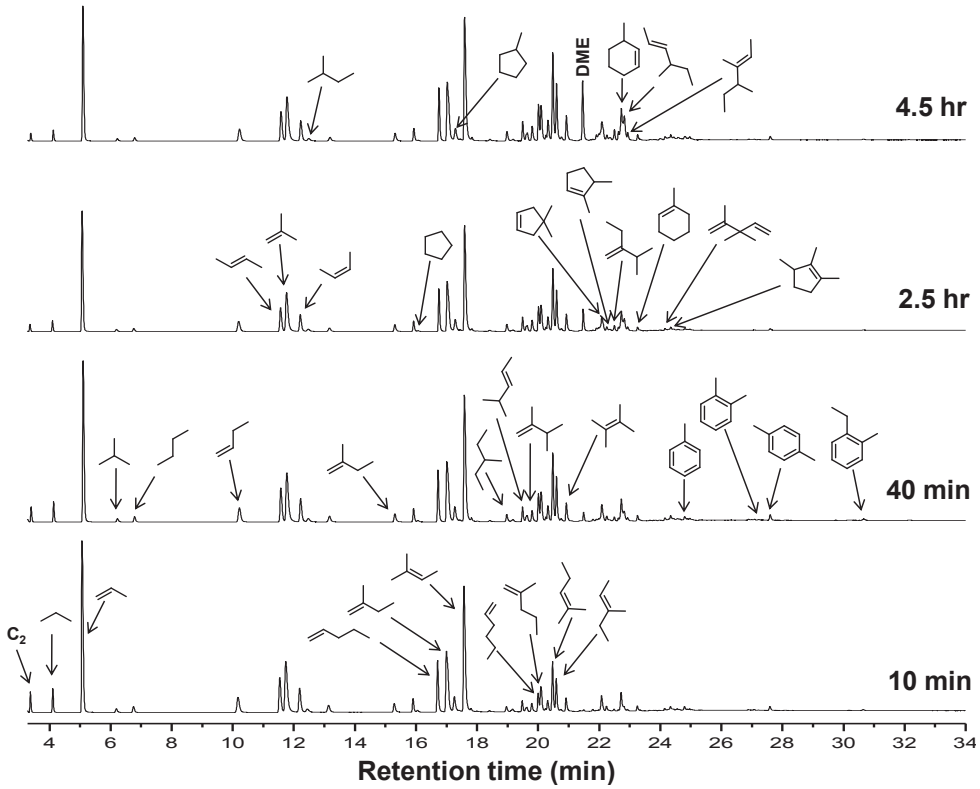

Figure 4.2: GC-MS total ion chromatogram of the MTH reaction effluent over ZSM-22 after different time on stream (TOS). Reaction carried out at 400^{o}C and WHSV = 2. $gg^{-1}h^{-1}$.

Figure 4.1 (right panel) together with Figure 4.2 displays product distribution of the MTH reaction over ZSM-22 as a function of time on stream at 400 °C and WHSV = 2 $gg^{-1}h^{-1}$. Selectivity towards C_3 (mostly propene) was highest initially and decreased with increasing

deactivation. There was a gradual decrease in the C_4 and C_5 selectivities with deactivation. A remarkable increase for the C_6+ fraction was observed with progressive catalyst deactivation. Notably, very little C_2 is formed and very high selectivity towards branched C_5+ hydrocarbons and negligible amounts of aromatics were detected. The product distribution observed over ZSM-22 is an intermediate between MTO (mainly C_2 and C_3) and MTG (rich in aromatics) processes, which potentially provides product flexibility in MTH applications. The C_5+ fraction was closely inspected, and branched alkenes were the most abundant (~70 %). Ideally, gasoline should consist of branched alkanes with mainly five to ten carbon atoms and there are limits on aromatic content [5]. Interestingly, these requirements can be met by hydrogenation of the MTH reaction products over ZSM-22 catalyst and might be suitable as environmentally friendly gasoline. Alternatively, the alkene rich product might be utilized as an alkylation feedstock to increase the carbon number in addition to provide saturation.

Optimizing shape selectivity: ZSM-22 displays high selectivity towards C_5+ hydrocarbons with negligible amounts of aromatics. These hydrocarbons fall in the boiling range of gasoline fuel. Hence, one can refer to the conversion of methanol over ZSM-22 as an MTG process, in which synthetic gasoline is produced from methanol with by-product C_2-C_4 hydrocarbons. By-product formation decreases the efficiency of chemical processes. One way of reducing the amount of by-products is by applying recycling. In this section, the effect of recycling of light hydrocarbons (C_2-C_4), that are undesired in gasoline fuel, is elucidated over ZSM-22 catalyst. Our laboratory setup does not allow the actual separation and recycling of light hydrocarbons formed during methanol conversion reactions. Therefore, other sources of hydrocarbons are added as co-reactants with methanol to simulate the actual recycling. Ethene, propene and butene were used as co-reactants that were formed *in situ* over the catalyst from ethanol, isopropanol and tert-butanol respectively.

Figure 4.3 displays methanol or methanol/alcohol mixtures conversion over ZSM-22 catalyst as a function of time on stream (left panel), and total methanol conversion capacities (right panel) of the various reactions. For the co-conversion studies, methanol conversion is calculated using the total area of oxygenate only, as described in section 3.2. As seen from Figure 4.3 (left panel), the catalytic performance of ZSM-22 is improved on adding alkenes to the reactant mixture. A systematic improvement in the catalyst's lifetime with the adding/recycling of the alkenes was observed in the order ethene < propene < butene. Previous kinetic studies of the reaction of methanol with light alkenes over ZSM-5 reported that the rate of methylation of the alkenes with methanol increases in the order ethene <

propene ≤ butene [107]. Interestingly, the improvement in catalyst performance during the co-conversion reaction shows a similar trend as methylation barriers. This suggests that, co-reacting of hydrocarbons with a lower methylation barrier will yield a greater improvement in the catalyst's performance.

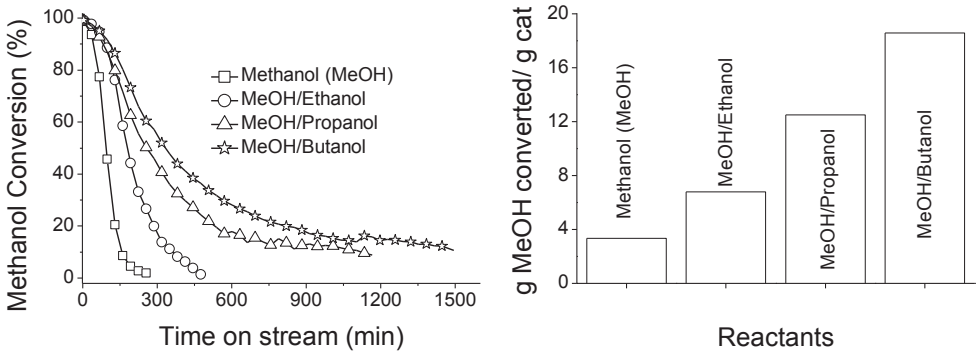

Figure 4.3: Catalyst deactivation profiles for a pure methanol feed and methanol co-fed with various alcohols (left panel), and total methanol conversion capacities for each of the aforementioned feeds (right panel) over ZSM-22 catalyst. Reaction carried out at 400 °C and WHSV = 2 $gg^{-1}h^{-1}$. The ratio of partial pressure of methanol to alcohol was kept at 10.4.

Figure 4.3 (right panel) displays the total methanol conversion capacities of the various reactions over ZSM-22, measured as gram methanol converted per gram catalyst before compete deactivation [108]. It is calculated by integrating the area under the conversion curve and extrapolating to zero conversion. Clearly, increased total methanol conversion capacities by factor of ~2, ~3.7 and ~5.6 were observed when adding ethanol, isopropanol and tert-butanol respectively. Zeolite based methanol conversion using a fixed bed reactor is reported to have zone ageing along the catalyst bed, and in some cases the very first layer of the catalyst bed is almost inert towards methanol conversion [109-111]. A possible explanation for the improved catalytic performance of ZSM-22 during co-conversion studies is that alkene methylation induces activation in the beginning of the catalyst bed, thereby extending the lifetime and conversion capacity of the catalyst bed as a whole. It should be noted that the total methanol conversion capacity for the commercial ZSM-22 catalyst used for the co-conversion studies is lower than our in-house synthesized materials (that vary between 6 and 12). The reason for this is unclear, but the observed increased lifetime during alkene co-reaction is clear and reproducible for this catalyst. Overall, the co-conversion studies suggest that recycling of light hydrocarbons during the MTH process over ZSM-22 will increase the stability of the catalyst towards deactivation, which results in an improved total methanol conversion capacity.

The effect of recycling on the product distribution is highlighted using propene (propanol) as an example, Figure 4.4. The result is presented as product yield when methanol is reacted and as reactor outlet composition when methanol and propene are reacted. Three major features were observed. First, at very high methanol conversions, small differences were observed between the product yields and the reactor outlet compositions. This suggests that at high methanol conversions, the co-added propene is converted to various hydrocarbons, and the product distribution of the MTH reaction remains mostly unchanged upon addition of propene at high methanol conversions.

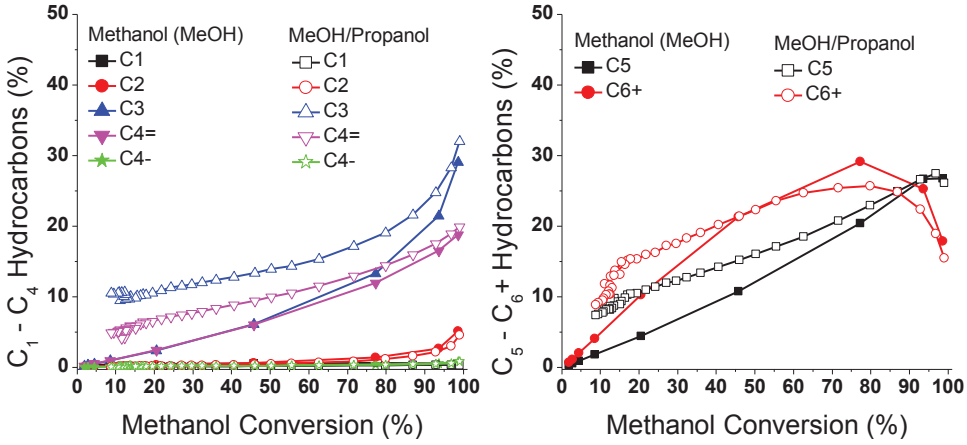

Figure 4.4: Product yield during methanol conversion (closed symbols) and reactor outlet composition during co-conversion of methanol with propanol (open symbols) as a function of methanol conversion over ZSM-22 catalyst at 400 °C. Partial pressure of methanol to isopropanol = 104.4 hPa.

Second, with increasing deactivation the difference between the product yields and reactor outlet compositions increased. This difference is mainly noticed in C_4 and C_5+ hydrocarbons. This suggests that methylation reactions are favored with increasing deactivation. Third, the amounts of propene detected in the outlet composition was much less than the amounts of propanol the feed, indicating that there is a net conversion of the added propene to hydrocarbons. Overall, the results suggest that if propene is recycled it will be converted to various hydrocarbons, and higher alkenes are formed via methylation reactions.

An isotopic labeling experiment was performed using ^{13}C methanol and ^{12}C isopropanol. Figure 4.5 displays the isotopic composition of butene. At high methanol conversion, majority of the butenes were either fully labeled or consist 1 × ^{13}C atoms. The former is ascribed to reaction of methanol and other hydrocarbons that do not have ^{12}C atoms, and the later is ascribed to single methylation of the co-added ^{12}C propene with ^{13}C methanol.

With increasing deactivation a significant increase of the singly labeled butene was observed, showing that methylation of ^{12}C-propene to butene is favored at lower conversion (low contact times). Similar results were obtained for double and triple methylation, i.e. pentene and hexene respectively. The result shows that the added propene molecules are methylated and their carbon number increased towards acceptable gasoline range hydrocarbons.

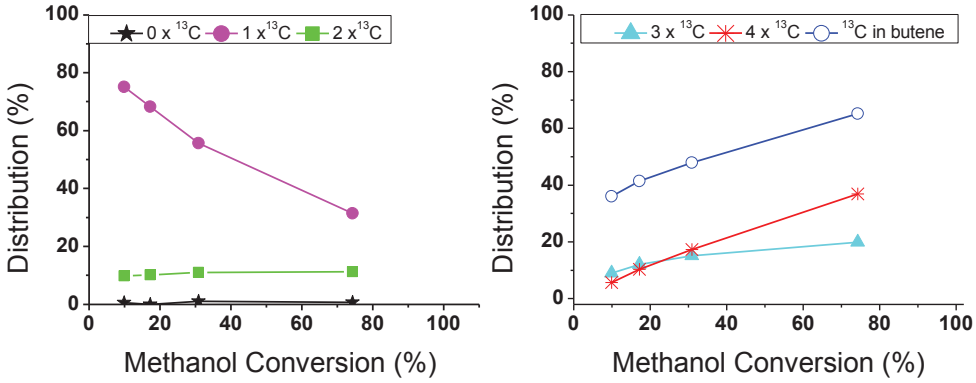

Figure 4.5: Isotopic composition of butene as a function of methanol conversion

Similar product distribution results were observed when adding ethene and butene as co-reactants (not shown here). Overall, the result suggests that recycling of the light hydrocarbons during the conversion of methanol over ZSM-22 will not significantly change the product distribution and yield as compared to a pure methanol feed. Furthermore, isotopic composition analysis when co-reacting all the alcohols indicates that, at very high methanol conversion the ^{13}C atoms are fully scrambled into the products. However with increasing deactivation, a clear systematic single, double or even triple methylation of the co-reacted alkene with methanol is observed. This result is in agreement with the reduced amount of the co-reacted alkene in the reactor outlet, and shows a net conversion of the alkenes. Thus, the co-conversion studies show that the by-products in the MTG process over ZSM-22 can be recycled and used as co-reactants with methanol, which results in further conversion of the by-products to various hydrocarbons of similar type as the one obtained from methanol. Such use of by-product as co-reactants will improve the efficiency of the process, and a higher amount of the desired hydrocarbons is obtained.

Reaction mechanism influencing shape selectivity: Clearly, ZSM-22 is an active catalyst for the conversion of methanol to hydrocarbons. The MTH reaction mechanism has been extensively studied over SAPO-34, ZSM-5 and Beta zeolites, and details on the mechanism are provided in section 2.2. Briefly, the MTH reaction is believed to proceed

through an indirect path rather than direct coupling of C_1 units. The indirect mechanism involves hydrocarbons within the zeolite pores as reaction centers, often referred to as hydrocarbon pool species. Investigations of the identity of the hydrocarbon pool species over catalysts such as ZSM-5, SAPO-34 and Beta have revealed that polymethylbenzenes (methylated benzene molecules) act as reaction centers during methanol conversion [62-65]. The alkenes formed from the hydrocarbon pool are controlled by the identity of the methylbenzene intermediate involved. For Beta higher methylbenzene intermediates favor the formation of propene and butenes [67], and for ZSM-5 catalyst lower methylbenzene intermediates favor the formation of mainly ethene and some propene [71].

Recent reexamination of the MTH reaction mechanism over ZSM-5 by Svelle et al. [62, 66], have clearly shown that the MTH reaction mechanism varies with pore architecture. Both alkene and aromatics were investigated as reaction centers operating simultaneously. This finding led to the introduction of the dual cycle concept [62] (Illustrated in section 2.2, scheme 2.4). The aromatic based reaction path is in agreement with the generally accepted hydrocarbon pool mechanism [57-59] (Illustrated in section 2.2, scheme 2.2), and the alkene based path is in agreement with the scheme originally proposed by Dessau [60, 61] (Illustrated in section 2.2, scheme 2.1). During the introduction of the dual cycle concept, the authors raised the interesting question whether one of the cycles can run independently and if it could be possible to manipulate the relative contribution from these cycles to the product formation, thereby controlling the selectivity. Therefore, we found it interesting to investigate the MTH reaction mechanism over ZSM-22 zeolite due to the narrow channels of the material that are likely to suppress the space demanding aromatic based reaction mechanism.

Isotope switching experiments from ^{12}C methanol to ^{13}C methanol were used to investigate the reaction mechanism over ZSM-22 catalyst as described in section 3.3. Figure 4.6 shows total ^{13}C contents in the alkenes and retained material after 2 min (left panel), 5 min (middle panel) and 18 min (right panel) of ^{12}C methanol reaction followed by 0.5, 1 and 2 min of ^{13}C methanol reaction over H-ZSM-22 at 400 °C, WHSV = 2 $gg^{-1}h^{-1}$ at full conversion. Clearly, a much faster incorporation of ^{13}C was observed in the effluent alkenes than in the retained materials. For the switching performed after 18 minutes of ^{12}C reaction the retained hydrocarbons are virtually inert for ^{13}C incorporation. In contrast, the total ^{13}C content in the effluent alkenes is notability high, which indicates that most of the alkenes are reactive to the incoming methanol than the retained hydrocarbons. The result clearly shows that the alkene based mechanism can operate more or less independently over ZSM-22. Unlike ZSM-5, SAPO-34, and Beta, the aromatic-based cycle is almost not in operation. Similarly, for the

switching performed after 2 and 5 minutes of ^{12}C methanol reaction the retained hydrocarbons displayed low reactivity towards the incoming ^{13}C methanol. However, compared to the switching after 18 minutes the switching performed after 2 or 5 minutes of ^{12}C reaction showed higher amounts of total ^{13}C. One contribution for this observation is the formation of retained hydrocarbons exclusively from ^{13}C methanol. These findings were later reproduced by Le et al. at 450 °C [112, 113].

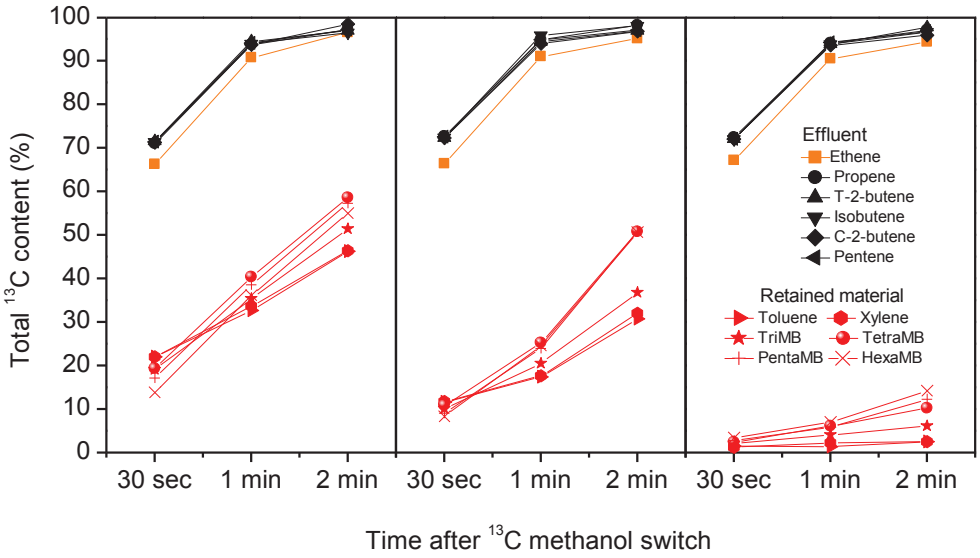

Figure 4.6: Total ^{13}C contents in the alkenes and retained material after 2 min (left panel), 5 min (middle panel) and 18 min (right panel) of ^{12}C methanol reaction followed by 0.5,1 and 2 min of ^{13}C methanol reaction over ZSM-22 at 400 °C, WHSV = 2 $gg^{-1}h^{-1}$ at full conversion.

Figure 4.7 displays GC-FID chromatograms of the gas phase effluent of the MTH reaction over SAPO-34, ZSM-22, Beta and ZSM-5 catalysts at 400 °C and WHSV = 2 $gg^{-1}h^{-1}$. SAPO-34 gives mainly C_2 and C_3, while ZSM-5 and Beta display product spectra with clear peaks in the aromatic region. Compared to the rest of the materials in which the aromatic based hydrocarbon pool mechanism is operational, the product distribution over ZSM-22 has the lowest amount of C_2, and negligible amount of aromatics and alkanes. Importantly, propene and higher alkenes, which are the major products of alkene based reaction path, are selectively produced over ethene and alkanes/aromatics. The isotope switching studies over ZSM-22 clearly shows that the nature of the MTH reaction mechanism determines the product selectivity, demonstrating the possibility of controlling the shape selectivity of zeolites through fundamental mechanistic insight. By carefully choosing a catalyst topology with narrow pores that suppresses space demanding aromatic based mechanism, product

formation via alkene based reaction cycle is favored. As a result, C_3+ hydrocarbons are selectivity produced over aromatics, alkanes and C_2.

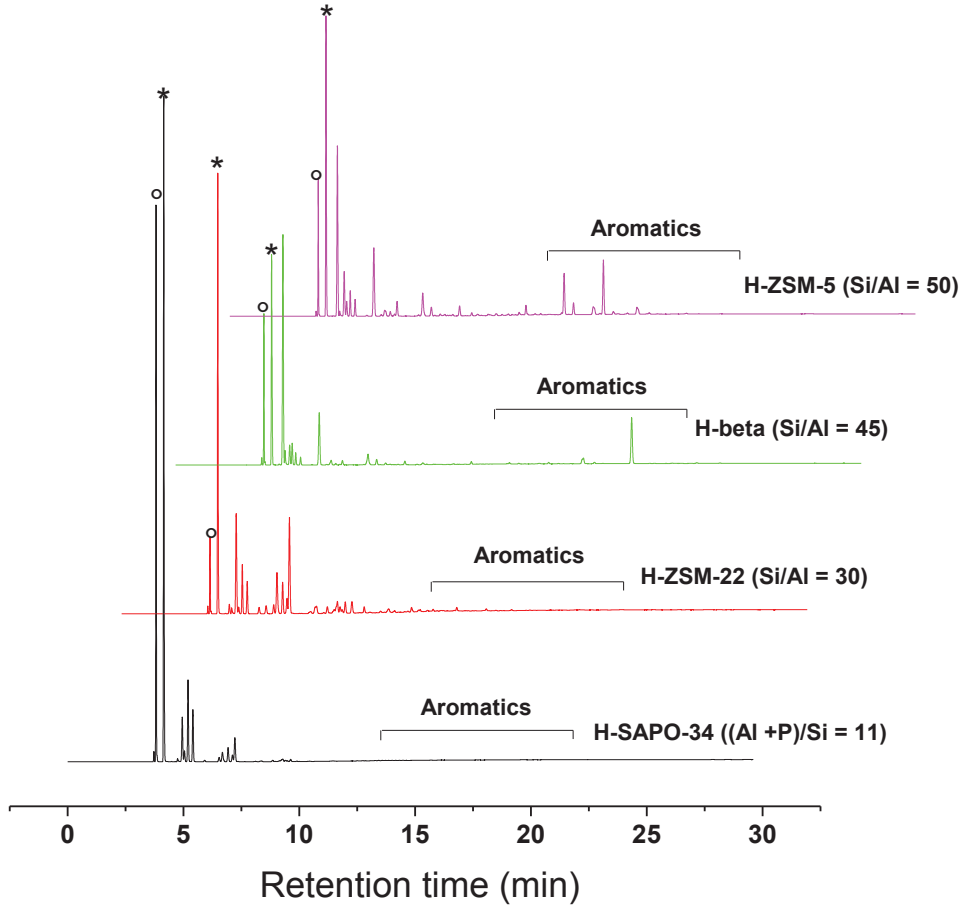

Figure 4.7: GC-FID chromatograms of the gas phase effluent of the MTH reaction over SAPO-34, ZSM-22, Beta and ZSM-5 catalysts at 400 °C and WHSV = 2 $gg^{-1}h^{-1}$.

Sensitivity of shape selectivity: Shape selectivity and diffusion in zeolite catalysis can be susceptible to subtle changes in catalyst topology and reactant or product molecules. Csicsery [35] states that if the dimensions of the reacting molecules approaches the dimensions of the pores, even subtle changes in the dimensions or configurations of the reacting or product molecules can cause a large difference in the diffusivities and reactivity of molecules. The most common example given to emphasize this is the diffusivity of para-xylene in ZSM-5 which is an order of magnitudes faster than the other two isomers [35, 114]. Other one-dimensional 10-ring zeolites with dimensions comparable to ZSM-22 catalyst exist.

Investigations of such systems will provide further understanding of the effect of subtle changes in pore sizes and shapes on the shape selectivity of one-dimensional 10-ring zeolites. Furthermore, ZSM-22 is a promising catalyst for production aromatic free gasoline, but compared with other catalysts and ZSM-5 in particular, the stability of the ZSM-22 toward deactivation is lower [90, 96]. Hence, other one-dimensional 10-ring zeolite having comparable channels sizes as ZSM-22 are tested for the MTH reaction under similar conditions.

Catalysts ZSM-22 (elliptical, 5.7 × 4.6 Å), ZSM-23 (teardrop, 5.2 × 4.5 Å), EU-1 (zig-zag, 5.5 × 4.1 Å), and ZSM-48 (cylindrical, 5.6 × 5.3 Å) were studied, illustrated in Figure 4.8. The catalysts have comparable 10-ring channels but they are different in channel shape. Moreover, ZSM-23 and EU-1 zeolites have small and large pore extensions (side pockets) respectively. The side pocket in EU-1 is 6.8 × 5.8 × 8.1 Å in dimensions [38]. The materials may be viewed as a series of catalysts with very similar one dimensional 10-ring pores with perpendicular extensions or side pockets of sizes increasing in the order ZSM-48 ≤ ZSM-22 < ZSM-23 < EU-1. Alternatively, the materials may be ranked according to the largest distance/opening giving rise to the series ZSM-23 ≤ ZSM-22 < ZSM-48 < EU-1.

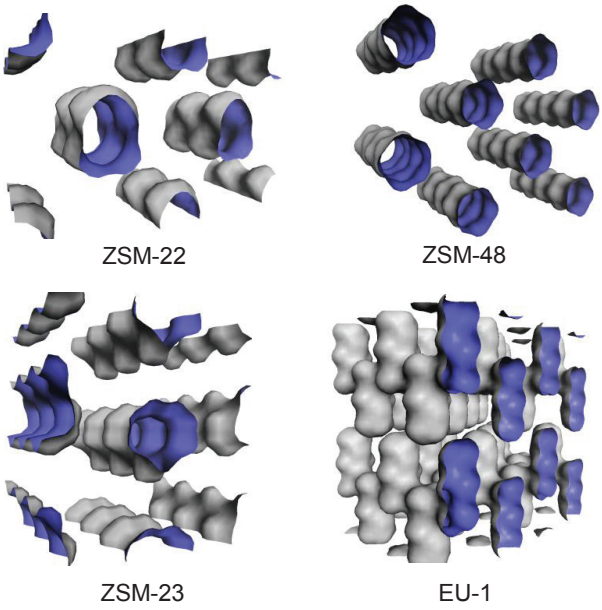

Figure 4.8: Illustrations of channel systems of ZSM-22, ZSM-23, ZSM-48 and EU-1

The synthesis of the zeolites is described in section 3.1 and Refs. [78, 82, 83]. The catalysts were characterized using SEM, NH_3-TPD, XRD and N_2-sorption. The Si/Al ratios of the catalysts, as determined from NH_3-TPD, are within a limited range of 30-52. XRD revealed that, except from an insignificant amount of a dense phase in ZSM-22 [80, 81], the catalysts are single phase and crystalline. All materials exhibit acceptably high BET surface areas and particle sizes ranging from <1 to 2-3 μm. All the characterization results are in agreement with the previous reports over the materials, and as expected for zeolite catalysts [83, 84, 115-126]. On the basis of these similarities, it appears reasonable to assign major differences in shape selectivity to differences in topologies.

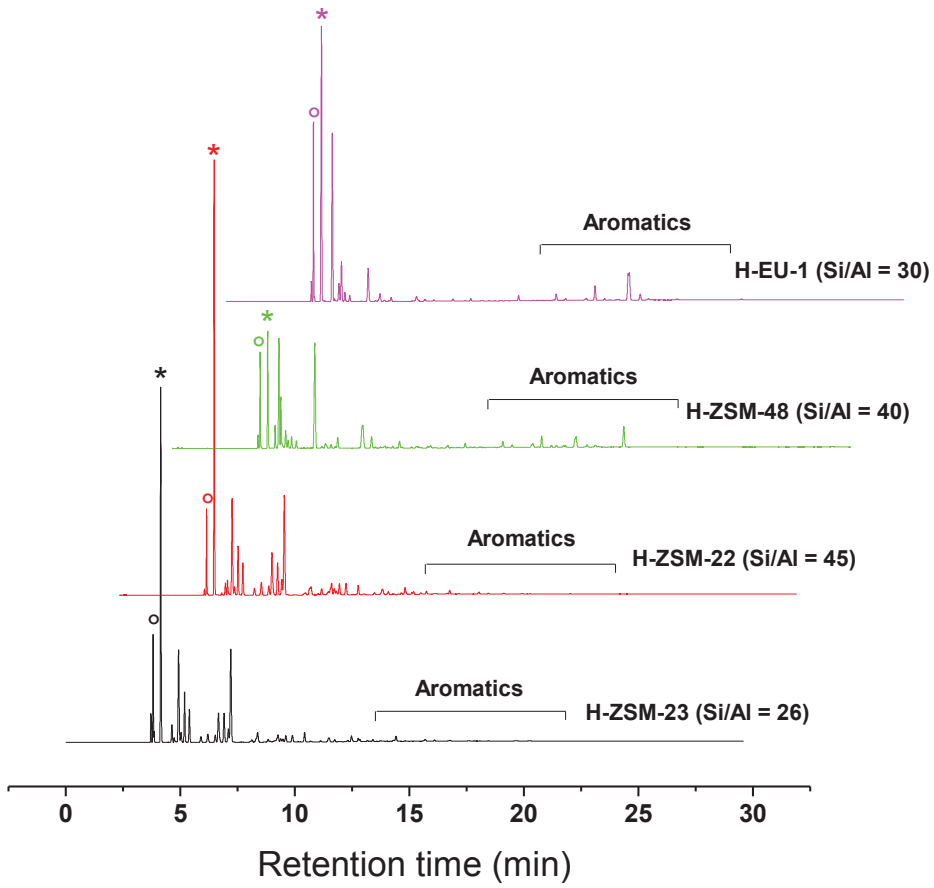

Figure 4.9: GC-FID chromatograms of the gas phase effluent of the MTH reaction over ZSM-22, ZSM-23, ZSM-48 and EU-1 catalysts at 400 °C and WHSV = 2 $gg^{-1}h^{-1}$

Figure 4.9 displays GC-FID chromatograms of the gas phase effluent of the catalysts obtained during the MTH reaction under identical test conditions, 400 °C and WHSV = 2 gg-

$^{1}h^{-1}$. At these conditions, the catalysts gave nearly full conversion, except ZSM-48, for which a conversion of 88% was achieved. Clearly, ZSM-22 and ZSM-23 displayed very similar product distribution, without noticeable amounts of aromatic compounds. By comparing the pore shape of ZSM-22 and ZSM-23, the very small side pockets of ZSM-23 did not influence the product distribution of the MTH process. The ZSM-48 catalyst displayed a product spectrum comprising substantial amounts of aromatics. This observation might be ascribed to the wider channels of the ZSM-48 catalyst relative to ZSM-22 and ZSM-23. Clearly, subtle increase in channel size significantly changed the product distribution. Similar to the previous report on the material, EU-1 which has the narrowest 10-ring channel, displayed a product spectrum comprising of aromatic compounds [110]. A plausible explanation for this unexpected product distribution over EU-1 zeolite might be the involvement of the 12-ring side pockets on the outer surface of the crystal during the MTH reaction, a similar phenomenon was addressed for MCM-22 zeolite previously [91, 127-130]. The results from the one-dimensional 10-ring zeolites show that the shape selectivity of zeolites is influenced by subtle variations in pore size and shape. By comparing the product distribution over ZSM-48 with that of ZSM-22 and ZSM-23, it is clear that the diffusion of aromatics is enhanced over ZSM-48 due to the slightly bigger channels. Furthermore, the detected aromatics in the gas effluent of EU-1 suggest contribution of pore extensions to the reaction, displaying unexpected product distribution. The materials have comparable stabilities towards deactivation at their optimum MTH conditions.

Coke and shape selectivity: Building up of coke species is the main cause for deactivation of zeolites during hydrocarbon conversion reaction [62, 131-133]. In addition, with progressive deactivation of catalysts due to coking, changes in product distributions are often observed. For example, a remarkable increase in C_6+ fraction is observed over ZSM-22 with increasing deactivation. This change might be linked to several parameters such as formation accumulation of coke within the pores, which might change the diffusivity of molecules in the zeolite, pore structure, acid site density, distribution or acid site strength etc [134]. Previous studies of the MTH reaction over ZSM-5 catalysts highlighted that the change in product distribution with deactivation may be described as a continuous change in contact time due to a gradual loss of acid sites caused by coking during the reaction [135]. Recently, detailed work dedicated to such investigations have revealed that coke deposition does not change shape selectivity of ZSM-5 catalyst during the MTH reaction [109]. The relationship between coke depositions and changes in shape selectivity is not obvious over one-

dimensional 10-ring zeolites, for which one could expect changes in diffusion properties due to pore blocking. Hence, the influence of coke deposition on the selectivity of ZSM-22, EU-1 and ZSM-23 zeolites was examined. In-house synthesized (ZSM-22 (H)) and commercially available (ZSM-22 (C)) ZSM-22 catalysts were investigated. The investigation has been carried out by changing the contact times (WHSV) of the reaction so that a certain level of conversion is reached corresponding to different degree of coking [134, 135].

Figure 4.10 displays yield versus conversion curves during the MTH reaction over the catalysts at 400 °C and different space velocities are indicated using different colors, WHSV = 2 (black), 3 (red), 4 (green), 5 (blue) and 6 (pink) $gg^{-1}h^{-1}$.

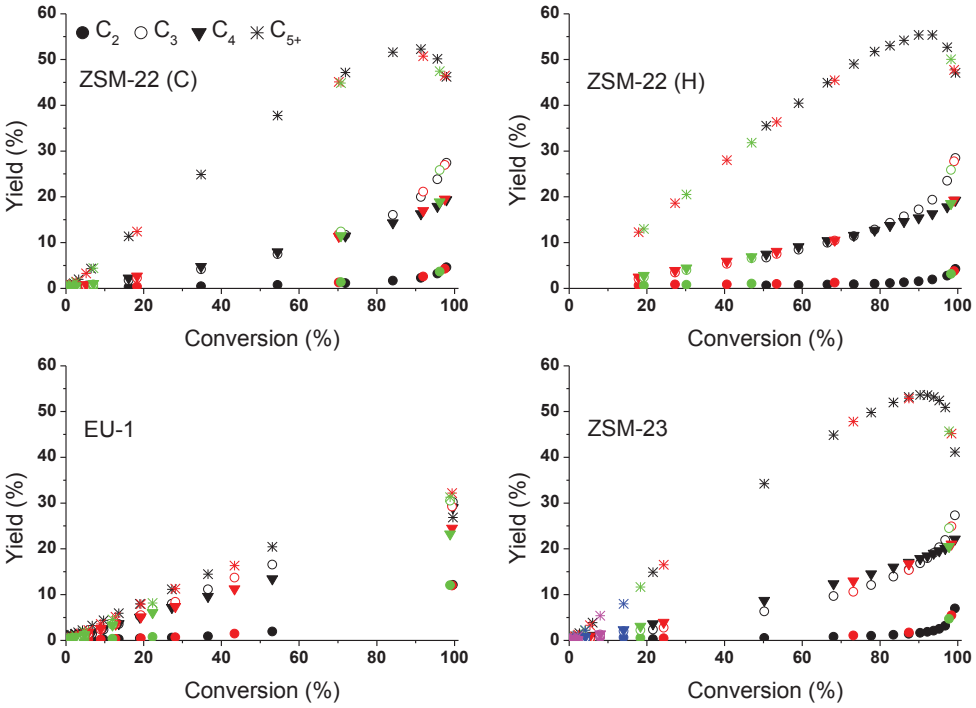

Figure 4.10: Yield (C%) as a function of methanol conversion (%) during the MTH reaction over ZSM-22 (C) (top left panel) ZSM-22 (H) (top right panel), ZSM-23 (bottom left panel) and EU-1 (bottom right panel) catalysts. Reactions carried out at 400 °C and WHSV = 2 (black), 3 (red), 4 (green), 5 (blue) and 6 (pink) $gg^{-1}h^{-1}$. Yield for methane is not included as it is very small

The influence of coke on the selectivity may be described using the ZSM-23 catalyst as a representative example. The initial conversion at WHSV = 6 $gg^{-1}h^{-1}$ over the fresh ZSM-23 catalyst was ~10 %, that is after feeding only 0.1 gram methanol per gram of catalyst. Whereas at WHSV = 2 $gg^{-1}h^{-1}$, 14 gram of methanol per gram of catalyst was fed before the conversion dropped to ~10 %. Interestingly, the observed yield at ~10 % conversion over the

fresh catalyst at WHSV = 6 $gg^{-1}h^{-1}$ and coked catalyst at WHSV = 2 $gg^{-1}h^{-1}$ were very similar. In the same manner, the amount of coke at all the space velocities (WHSV = 2, 3, 4 and 6 $gg^{-1}h^{-1}$) were different, but similar yields were found at a given conversion. These data strongly suggest that the yield at a certain conversion level is independent of the amount of coke deposited. Thus, the change in selectivity with time on stream can be regarded as a change in contact time. This holds also when the MTH reaction is carried out over EU-1 and ZSM-22 catalysts. Such behavior has been referred to as nonselective deactivation by Chen et al. [134]. In contrast, selective deactivation was demonstrated for the MTO reaction over SAPO-34, coke deposition resulted in changes in shape selectivity [134]. The conclusion derived from Figure 4.10, i.e. that for a given catalyst sample, the product distribution may be described solely as a function of conversion and appears to be independent of the degree of coking, implies that shape selectivity of the materials is not changed by coke depositions. The major consequence of such an observation is that deactivation modeling [135] and single event kinetic modeling[a] of the MTH reaction over ZSM-22, ZSM-23 and EU-1 zeolites could be achieved by minor modification of models already developed for ZSM-5.

Morphology and shape selectivity: As presented in the previous sections, investigation of shape selectivity in zeolites requires several experiments involving synthesis, characterization and catalytic tests. According to the international zeolite association (IZA), there are more than 200 zeolite structures and these structures are a very small fraction of the millions of structures feasible on theoretical grounds [136]. Efforts to match novel and existing zeolite structures with new or improved applications requires both optimum tools and concise concepts to indentify zeolite catalysts suitable for the desired applications in predictable manner. Smit and Maesen [6] stated that computer simulation will provide valuable information on the detailed mechanistic insights into the nucleation and crystal growth of zeolites that might eventually allow us to rationally choice zeolites that are suitable for particular applications. Here, we highlight the importance of particle morphology as a tunable parameter giving rise to shape selectivity. This finding is presented using SUZ-4, SAPO-34, ZSM-22 and ZSM-5 catalysts.

SUZ-4 (SZR topology) has a three-dimensional pore system consisting of medium (10-ring, 4.1 × 5.2 Å, viewed along [001]) and small (8-ring, 4.8 × 3.0 Å, viewed along [110] and 4.8 × 3.2 Å, viewed along [010]) pores. The SUZ-4 catalyst was synthesized following the procedures in Refs. [86, 137]. SAPO-34 is a small pore MTO catalyst, while ZSM-5 is a medium pore MTG catalyst. ZSM-22 is a medium pore catalyst, with an intermediate product

[a]Kumar et al. *Ind. Eng. Chem. Res.*, , *52* (**2013**), 1491–1507

distribution between MTO and MTG. The topology of SUZ-4 contains some of the structural elements of SAPO-34, ZSM-5 and ZSM-22 and it is therefore interesting to investigate how the material behaves in terms of shape selectivity during the MTH reaction. All the catalysts were tested for the MTH reaction under similar conditions, 400 °C and WHSV = 2 $gg^{-1}h^{-1}$.

Figure 4.11 shows the product distribution of the MTH reaction over ZSM-5, ZSM-22, SUZ-4 and SAPO-34 catalysts, at 400 °C and WHSV = 2 $gg^{-1}h^{-1}$. Over ZSM-5 (Si/Al = 50) and ZSM-22 (Si/Al = 30) catalysts, the majority of the product formed is C_4+ hydrocarbons. This is as expected from medium pore zeolites. On the other hand, SUZ-4 (Si/Al = 8) and SAPO-34 ((Al+P)/Si = 11) catalysts displayed products rich in light hydrocarbons (C_2 and C_3). The selectivities towards C_2 + C_3 hydrocarbons are 72.2 % and 62.1 %, while the C_4+ selectivities are 27.2 and 27.7 % over SAPO-34 and SUZ-4 respectively. It should be noted that the amount of methane is higher over SUZ-4, which is due to the high acid site density that resulted in rapid deactivation of the catalyst (fully deactivated after 30 minutes on steam).

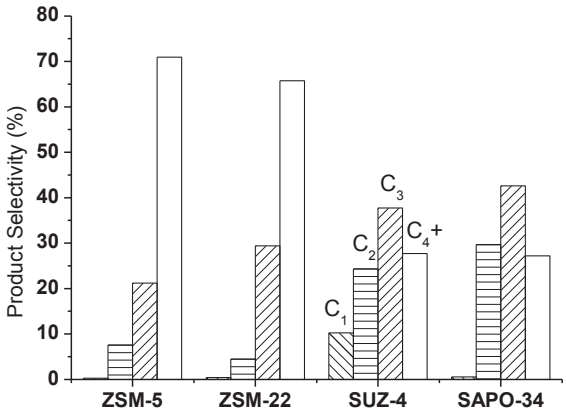

Figure 4.11: MTH product over ZSM-5, ZSM-22, SUZ-4 and SAPO-34 catalysts

We also tested SUZ-4 at temperatures 350 °C (83 % methanol conversion) and 450 °C (near full methanol conversion), and similar results were obtained. Despite the presence of 10-ring channels in the framework, the shape selectivity of SUZ-4 is very similar to SAPO-34, for which the 8-ring windows control the diffusion of molecules. To shed light on this surprising behavior, it is important to know how the topology of the SUZ-4 material is embedded into the crystal morphology. Below we present computational morphology prediction, TEM imaging, selected area electron diffraction (SAED) and X-ray diffraction analysis, which together reveal that the shape selectivity of SUZ-4 is induced by its crystal morphology.

***Morphology prediction*:** Morphology of a crystalline material reflects the internal arrangement of atoms in the crystal, which is an extended arrangement of atoms in the unit cell. One of the common and a quick approach for predicting crystal morphology is the Bravais-Friedel Donnay-Harker (BFDH) method [138]. The method uses crystal lattice and symmetry of the unit cell to identify the growing faces and predict their relative growth rates. According to the BFDH theory, the relative growth rate of a plane is inversely proportional to the interplanar distance *d* spacing, and the morphologically important planes are those with the biggest *d* spacing. The BFDH model as implemented in the Materials Studio software simulation suits was used to simulate the growth of SUZ-4.

Figure 4.12 displays the morphology of SUZ-4 generated from prediction using the BFDH model, and a magnified part illustrating the channel orientation within the crystal. The growth directions are indicated by the arrows and the growth rates are proportional to the arrow sizes. Two main conclusions can be drawn from the BFDH analysis. First, the crystal growth is highly anisotropic, with an enhanced growth along the *c* direction (Figure 4. 12, top), yielding a needle-like morphology. Second, the magnified region (Figure 4.12, bottom) shows that the 10-ring channels go along the crystallographic *c* direction, which is also the direction of the needle. This means that the 10-ring channels are only accessed from the edges of the needle-like crystal, while the 8-rings are perpendicular to the 10-ring channels, and therefore accessed from the sides of the needle-like crystal. Such orientation of the channels within the crystals will lead to a situation where the diffusion is likely to be controlled by the much shorter 8-rings, which at the same time cover most of the outer surface. The predicted morphology, would explain the observed selectivity during the MTH reaction over SUZ-4.

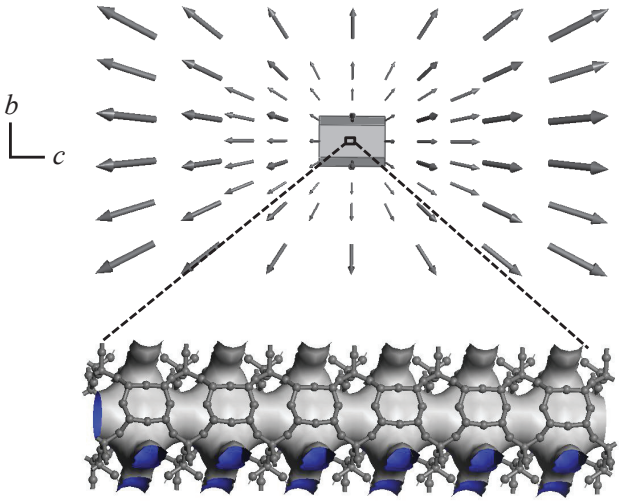

Figure 4.12: Predicted SUZ-4 crystal morphology using BFDH model (top), and arrangement of the 8-ring and 10-ring channels within the crystal (bottom)

***TEM imaging*:** To prove the prediction of the morphology and the channel orientation experimentally, TEM imaging and SAED were performed (description of the setup is previously provided [139]). Gold was used as internal diffraction standard to obtain exact lattice spacings. Figure 4.13 (left panel) displays a TEM image and the corresponding SAED pattern of the shown area (insert) of SUZ-4 crystallite. The characteristic feature of the particles is the distinct needle shape, which is in agreement with the elongated morphology predicted using the BFDH model. Such needle-like morphology was previously reported and appears to be favored [140].

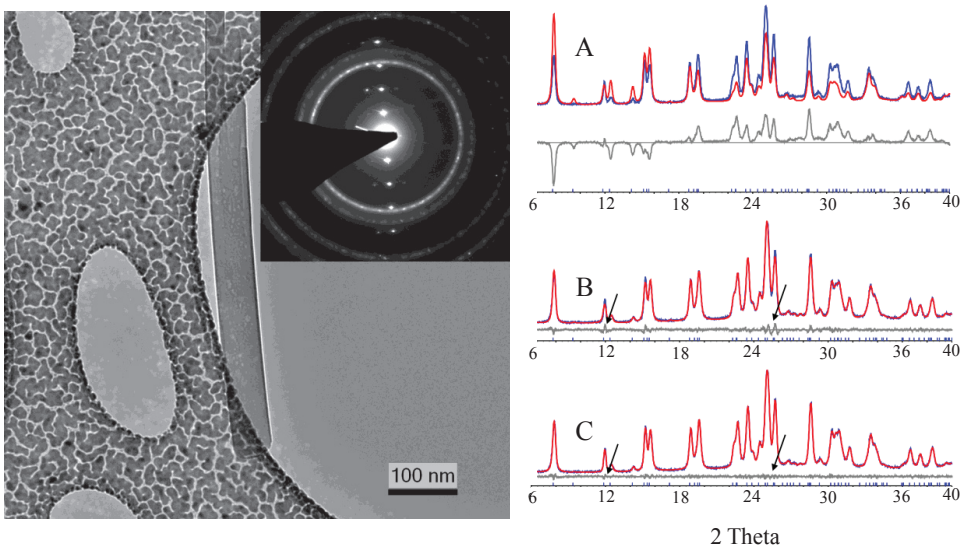

Figure 4.13: TEM image of a SUZ-4 crystal lying on gold coated lacy carbon film. The insert shows the selected area electron diffraction pattern of the shown area. The gold, seen as powder rings in the diffraction pattern, is used as internal diffraction standard for precise lattice parameter determination (right panel), and full profile powder data analysis. A) Rietveld analysis using SUZ-4 reference structure from the IZA database. B) Standard LeBail analysis. C) LeBail analysis combined with the ellipsoid formalism. The blue and the red curves are observed and model data respectively. The arrows highlight the improved fit of the model data to the observed data (left panel).

During the collection of electron diffraction data, the needle-like crystallites were mostly laying horizontally on the carbon film. Bragg spots in the direction of the needle were readily observed. Lattice spacings of ~7.46 Å that corresponds to the *c* axis of the unit cell were consistently observed. This confirms that the *c* direction of the unit cell runs in the direction of the needles. Once the *c* direction is correctly assigned, the 8-ring and 10-ring channels are readily determined i.e. the 10-ring channels are oriented along the *c* direction, and the 8-ring channels are perpendicular to it. Therefore, the TEM studies confirm a needle-like morphology, with access to the 10- and 8-ring pores through the ends or the sides of the

needle respectively. Overall, the TEM analyses were in agreement with the BFDH model, confirming that the shape selectivity of SUZ-4 is induced by its crystal morphology, not framework topology.

***Bulk analysis using PXRD*:** Figure 4.13 (right panel) shows powder X-ray diffraction data of SUZ-4 zeolite, collected on a Philips X'Pert (Cu K_α). The crystallinity and purity of the material is confirmed by Rietveld analysis (Figure 4A, Rwp = 33.28). The observed intensity discrepancy is caused by preferred orientation of the needle-like crystallites and an unknown amount of water in the zeolite channels. A LeBail fit results in a significantly better fit (Figure 4B, Rwp = 5.39), but the difference curve reveals anisotropy in peak broadening, which is related to the anisotropic morphology of the crystallites. Combining LeBail fitting with the ellipsoid formalism [139] results in a significantly improved fit (Figure 4C, Rwp = 3.69) and identifies the long needle direction as the short 7.46 Å crystal axis of SUZ-4 in agreement the BFDH model and the TEM/SAED analysis.

4.3. Main conclusions

- Unlike the previous reports, zeolite ZSM-22 is an active catalyst in the MTH reaction.
  - Low feed rates and temperatures in the range 400 - 500 °C are required for appreciable methanol conversion. The catalyst showed high selectivity towards branched aromatic free C_5+ hydrocarbons which could be used for the production of cleaner gasoline.
- Gasoline production from methanol over ZSM-22 can be improved by recycling of light alkenes.
- Alkene cracking/methylation mechanism controls the product selectivity during the MTH reaction over ZSM-22 catalyst.
  - By tuning the relative contribution of the alkene based and aromatic based mechanisms, formation of ethene, alkanes and aromatics are suppressed over ZSM-22, demonstrating the possibility of controlling the product selectivity based on intimate knowledge about the reaction mechanism for the conversion of methanol to hydrocarbons.
- Small differences in the channel system notably change the product distribution of the MTH reaction over one-dimensional 10-ring zeolites, ZSM-22, ZSM-23, ZSM-48 and EU-1.

- ZSM-22 and ZSM-23 give similar product distributions. The pores of ZSM-48 are big enough to allow the diffusion of aromatics that are detected in the gas phase effluent. The pore extensions (side pockets) of EU-1 are likely involved in the MTH reaction and give unexpected catalytic behavior.

- The change in the selectivities of the MTH reaction over ZSM-22, ZSM-23, and EU-1 zeolites with time on stream may be described as an effective reduction of contact time.
- The shape selectivity during the MTH reaction observed over SUZ-4 is induced by crystal morphology not framework topology.
  - SUZ-4 is an active catalyst for methanol conversion at temperatures between 350 and 450 °C. SUZ-4 crystallizes preferably with needle shaped morphology elongated in the *c* direction. The 10-rings of SUZ-4 zeolite are accessible only at the needle ends and the 8-rings cover the needle sides.

Suggestions for further work

One-dimensional 10-ring zeolites

The product distribution observed over the one-dimensional 10-ring zeolites is quite interesting. More specifically, ZSM-22 and ZSM-23 zeolites displayed high selectivity towards aromatic free gasoline range hydrocarbons. However, the stability of the catalysts towards deactivation compared to other catalysts, ZSM-5 in particular, is lower [90, 96]. Therefore, it would be interesting to continue the work towards understanding of the causes for the rapid deactivation of the materials and to carry out further work dedicated to prolonging the lifetime the materials. Improvements in the catalysts stability towards deactivation might be achieved by increasing the diffusion of molecules in the crystals. This can be addressed using two approaches, namely creation of mesopores and synthesis of the materials with shorter diffusion distances. Mesorpores can be created by desilication of zeolites, which often improve the catalysts lifetime [90]. Mesoporous ZSM-22 is previously reported [121], and similar studies might be adapted in continuation of this work. Similarly, the desilication work can also be extended to the other one-dimensional 10-ring zeolites. Recently, Ryoo and co-workers [131] synthesized nanosheets of ZSM-5 zeolite with improved resistance towards deactivation, primarily due to improved diffusion of molecules and coke precursors. Interestingly, ZSM-22 can be synthesized using 1,6-diaminohexane as structure directing agent [141], which is responsible for the templating effect in Ryoo's synthesis. Hence, the synthesis of ZSM-22 with nanometer thickness might be possible and that is likely to improve the catalyst's lifetime.

SUZ-4

The morphology induced shape selectivity over SUZ-4 can be an exciting research topic to investigate also other zeolites with pores of different sizes such as Offretite (OFF), which comprises linear 12-rings and perpendicular 8-rings, and several other materials [9, 12]. Furthermore, it would also be interesting to synthesize a series of SUZ-4 catalysts differing aspect ratios and morphologies and to evaluate the resulting product distributions, thereby providing a definitive and systematic relationship between morphology and shape selectivity.

The SUZ-4 catalyst used in this work deactivates rapidly. The main reason for this is the very high Si/Al ratio of the material for the MTH reaction. Hence, synthesis of SUZ-4 with Si/Al = 20 – 100 would be interesting topic in continuation of this work and it is likely to

prolong the lifetime of the material. Alternatively, one might improve the SUZ-4 stability towards deactivation by post synthesis removal of Al from the framework. Steaming of SUZ-4 might lead to such reduced amount of Al in the framework, which is reported as an effective post synthesis modification method for other zeolites [142-144].

References

(1) I. Chorkendorff, J.W. Niemantsverdriet, *Concepts of Modern Catalysis and Kinetics* Wiley-VCH: Weinheim, 2003.

(2) G.A. Somorjai, R.M. Rioux, *Catal. Today*, 100 (2005) 201-215.

(3) G.A. Somorjai, J.Y. Park, *Angew. Chem., Int. Ed.*, 47 (2008) 9212-9228.

(4) G.A. Somorjai, C.J. Kliewer, *React. Kinet. Catal. Lett.*, 96 (2009) 191-208.

(5) J.A. Moulijn, M. Makkee, A.V. Diepen, *Chemical Process Technology*. Jon Wiley and Sons: New York, 2001.

(6) B. Smit, T.L.M. Maesen, *Nature*, 451 (2008) 671-678.

(7) L.B. McCusker, F. Liebau, G. Engelhardt, *Pure Appl. Chem.*, 73 (2001) 381-394.

(8) J.X. Jiang, J.H. Yu, A. Corma, *Angew. Chem., Int. Ed.*, 49 (2010) 3120-3145.

(9) C. Baerlocher, L.B. Mccusker. *Database of Zeolite Structures: http://www.iza-structure.org/databases/*.

(10) A. Dyer, *An introduction to zeolite molecular sieves*. John Wiley and Sons Inc.: Chichester, 1988.

(11) J. Weitkamp, *Solid State Ionics*, 131 (2000) 175-188.

(12) W.M. Meier, D.H. Olson, C. Baerlocher, *Atlas of Zeolite Structure Types*. 5th ed.; Elsevier: Amsterdam, 2007.

(13) R.M. Barrer, *Pure Appl. Chem.*, 51 (1979) 1091-&.

(14) M.D. Foster, M.M.J. Treacy. *http://www.hypotheticalzeolites.net/*. [accessed 2012/14/11].

(15) Y. Li, J.H. Yu, R.R. Xu. *http://mezeopor.jlu.edu.cn/*. [accessed 2010/22/11].

(16) H. Robsen, K.P. Lillerud, *Verified Synthesis of Zeolitic Materials* 2nd ed.; Elsevier: Amsterdam, 2001.

(17) F. Di Renzo, *Catal. Today*, 41 (1998) 37-40.

(18) P.M. Slangen, J.C. Jansen, H. vanBekkum, *Microporous Materials*, 9 (1997) 259-265.

(19) K.E. Hamilton, E.N. Coker, A. Sacco, A.G. Dixon, R.W. Thompson, *Zeolites*, 13 (1993) 645-653.

(20) N.N. Feoktistova, S.P. Zhdanov, *Zeolites*, 9 (1989) 136-139.

(21) H. Kacirek, H. Lechert, *J. Phys. Chem.*, 79 (1975) 1589-1593.

(22) C.S. Cundy, P.A. Cox, *Microporous Mesoporous Mater.*, 82 (2005) 1-78.

(23) M.W. Ackley, S.U. Rege, H. Saxena, *Microporous Mesoporous Mater.*, 61 (2003) 25-42.

(24) R.E. Morris, *Angew. Chem., Int. Ed.*, 47 (2008) 442-444.

(25) A. Corma, L.T. Nemeth, M. Renz, S. Valencia, *Nature*, 412 (2001) 423-425.

(26) M.E. Davis, *Nature*, 417 (2002) 813-821.

(27) J.A. Rabo, M.W. Schoonover, *Appl. Catal., A*, 222 (2001) 261-275.

(28) A. Corma, *J. Catal.*, 216 (2003) 298-312.

(29) G.O. Brunner, W.M. Meier, *Nature*, 337 (1989) 146-147.

(30) A. Corma, *Chem. Rev.*, 95 (1995) 559-614.

(31) J.F. Haw, *Phys. Chem. Chem. Phys.*, 4 (2002) 5431-5441.

(32) G. Busca, *Chem. Rev.*, 107 (2007) 5366-5410.

(33) T.F. Degnan, *J. Catal.*, 216 (2003) 32-46.

(34) P.B. Weisz, *Pure Appl. Chem.*, 52 (1980) 2091-2103.

(35) S.M. Csicsery, *Pure Appl. Chem.*, 58 (1986) 841-856.

(36) M. Stöcker, *Microporous Mesoporous Mater.*, 29 (1999) 3-48.

(37) J.L. Schlenker, W.J. Rohrbaugh, P. Chu, E.W. Valyocsik, G.T. Kokotailo, *Zeolites*, 5 (1985) 355-358.

(38) N.A. Briscoe, D.W. Johnson, M.D. Shannon, G.T. Kokotailo, L.B. Mccusker, *Zeolites*, 8 (1988) 74-76.

(39) J. Kim, C.A. Henao, T.A. Johnson, D.E. Dedrick, J.E. Miller, E.B. Stechel, C.T. Maravelias, *Energy Environ. Sci.*, 4 (2011) 3122-3132.

(40) G.A. Olah, A. Goeppert, G.K.S. Prakash, *J. Org. Chem.*, 74 (2009) 487-498.

(41) C.D. Chang, *Cat. Rev. - Sci. Eng.*, 25 (1983) 1-118.

(42) C.D. Chang, A. J. Silvestri, *J. Catal.*, 47 (1977) 249-259.

(43) S.L. Meisel, J.P. Mccullough, C.H. Lechthaler, P.B. Weisz, *Chem. Tech.*, 6 (1976) 86-89.

(44) H. Ertl, F. Knözinger, F. Schüth, J. Weitkamp, *Handbook of Heterogeneous Catalysis*. 2nd ed.; Wiley-VCM: Weinheim, 2008; Vol. 6.

(45) J. Cobb, *New Zealand Synfuel: The Story of the World's First Natural Gas to Gasoline Plant*. Cobb/Horwood Publications: Auckland, New Zealand, 1995.

(46) F.J. Keil, *Microporous Mesoporous Mater.*, 29 (1999) 49-66.

(47) C.D. Chang, *Catal. Today*, 13 (1992) 103-111.

(48) J.Q. Chen, A. Bozzano, B. Glover, T. Fuglerud, S. Kvisle, *Catal. Today*, 106 (2005) 103-107.

(49) H. Koempel, W. Liebner, *Stud. Surf. Sci. Catal.*, 167 (2007) 261-267.

(50) M. Stöcker, *Microporous Mesoporous Mater.*, 82 (2005) 257-292.

(51) J. Topp-Jørgensen, *Stud. Surf. Sci. Catal.*, 36 (1988) 293-305.

(52) *http://www.uop.com/uop-technology-licensed-eurochem-convert-methanol-olefins-nigerian-petrochemicals-plant/*. [accessed 2012/07/11].

(53) U. Olsbye, S. Svelle, M. Bjørgen, P. Beato, T.V.W. Janssens, F. Joensen, S. Bordiga, K.P. Lillerud, *Angew. Chem., Int. Ed.*, 51 (2012) 5810-5831.

(54) http://www.exxonmobil.com/Apps/RefiningTechnologies/default.aspx. [accessed 2012/07/11].

(55) *http://www.uop.com/honeywells-uop-methanoltoolefins-technology-selected-convert-coal-highvalue-petrochemicals-china/*. [accessed 2012/07/11].

(56) W.G. Song, D.M. Marcus, H. Fu, J.O. Ehresmann, J.F. Haw, *J. Am. Chem. Soc.*, 124 (2002) 3844-3845.

(57) I.M. Dahl, S. Kolboe, *J. Catal.*, 161 (1996) 304-309.

(58) I.M. Dahl, S. Kolboe, *Catal. Lett.*, 20 (1993) 329-336.

(59) I.M. Dahl, S. Kolboe, *J. Catal.*, 149 (1994) 458-464.

(60) R.M. Dessau, R.B. Lapierre, *J. Catal.*, 78 (1982) 136-141.

(61) R.M. Dessau, *J. Catal.*, 99 (1986) 111-116.

(62) M. Bjørgen, S. Svelle, F. Joensen, J. Nerlov, S. Kolboe, F. Bonino, L. Palumbo, S. Bordiga, U. Olsbye, *J. Catal.*, 249 (2007) 195-207.

(63) Ø. Mikkelsen, P.O. Rønning, S. Kolboe, *Microporous Mesoporous Mater.*, 40 (2000) 95-113.

(64) B. Arstad, S. Kolboe, *J. Am. Chem. Soc.*, 123 (2001) 8137-8138.

(65) B. Arstad, S. Kolboe, *Catal. Lett.*, 71 (2001) 209-212.

(66) S. Svelle, F. Joensen, J. Nerlov, U. Olsbye, K.P. Lillerud, S. Kolboe, M. Bjørgen, *J. Am. Chem. Soc.*, 128 (2006) 14770-14771.

(67) S. Svelle, U. Olsbye, F. Joensen, M. Bjørgen, *J. Phys. Chem. C*, 111 (2007) 17981-17984.

(68) T. Mole, J.A. Whiteside, D. Seddon, *J. Catal.*, 82 (1983) 261-266.

(69) T. Mole, G. Bett, D. Seddon, *J. Catal.*, 84 (1983) 435-445.

(70) B.E. Langner, *Appl. Catal.*, 2 (1982) 289-302.

(71) M. Bjørgen, F. Joensen, K.P. Lillerud, U. Olsbye, S. Svelle, *Catal. Today*, 142 (2009) 90-97.

(72) A. Sassi, M.A. Wildman, H.J. Ahn, P. Prasad, J.B. Nicholas, J.F. Haw, *J. Phys. Chem. B*, 106 (2002) 2294-2303.

(73) A. Sassi, M.A. Wildman, J.F. Haw, *J. Phys. Chem. B*, 106 (2002) 8768-8773.

(74) D. Lesthaeghe, A. Horre, M. Waroquier, G.B. Marin, V. Van Speybroeck, *Chem. Eur. J.*, 15 (2009) 10803-10808.

(75) M. Bjørgen, U. Olsbye, D. Petersen, S. Kolboe, *J. Catal.*, 221 (2004) 1-10.

(76) M. Westgård Erichsen, S. Svelle, U. Olsbye, *J. Catal.*, in press (2012).

(77) R.F. Sullivan, R.P. Sieg, G.E. Langlois, C.J. Egan, *J. Am. Chem. Soc.*, 83 (1961) 1156-&.

(78) D. Masih, T. Kobayashi, T. Baba, *Chem. Commun.*, (2007) 3303-3305.

(79) M. Derewinski, M. Machowska, *Stud. Surf. Sci. Catal.*, 154 (2004) 349-354.

(80) R.M. Highcock, G.W. Smith, D. Wood, *Acta Crystallogr., Sect. C: Cryst. Struct. Commun.*, 41 (1985) 1391-1394.

(81) G.T. Kokotailo, J.L. Schlenker, F.G. Dwyer, E.W. Valyocsik, *Zeolites*, 5 (1985) 349-351.

(82) J. Shin, S.B. Hong, *Microporous Mesoporous Mater.*, 124 (2009) 227-231.

(83) S.H. Lee, C.H. Shin, D.K. Yang, S.D. Ahn, I.S. Nam, S.B. Hong, *Microporous Mesoporous Mater.*, 68 (2004) 97-104.

(84) G.L. Zhao, J.W. Teng, Y.H. Zhang, Z.K. Xie, Y.H. Yue, Q.L. Chen, Y. Tang, *Appl. Catal., A*, 299 (2006) 167-174.

(85) K. Suzuki, T. Hayakawa, *Microporous Mesoporous Mater.*, 77 (2005) 131-137.

(86) S. Jiang, Y.K. Hwang, S.H. Jhung, J.S. Chang, J.S. Hwang, T.X. Cai, S.E. Park, *Chem. Lett.*, 33 (2004) 1048-1049.

(87) A. Zecchina, G. Spoto, S. Bordiga, *Phys. Chem. Chem. Phys.*, 7 (2005) 1627-1642.

(88) J. Čejka, H. Van Bekkum, A. Corma, F. Schueth, *Introduction to Zeolite Science and Practice*. 3rd ed.; 2007; Vol. 168.

(89) P.O. Rønning, *Use of Isotopic Labelling in the Study of Methanol Conversion to Hydrocarbons over Zeolite H-ZSM-5*, 1998, Ph.D. Thesis, University of Oslo

(90) M. Bjørgen, F. Joensen, M.S. Holm, U. Olsbye, K.P. Lillerud, S. Svelle, *Appl. Catal., A*, 345 (2008) 43-50.

(91) M. Bjørgen, S. Akyalcin, U. Olsbye, S. Benard, S. Kolboe, S. Svelle, *J. Catal.*, 275 (2010) 170-180.

(92) M. Bjørgen, F. Bonino, S. Kolboe, K.P. Lillerud, A. Zecchina, S. Bordiga, *J. Am. Chem. Soc.*, 125 (2003) 15863-15868.

(93) U. Olsbye, S. Svelle, S. Aravinthan, M. Bjørgen, K.P. Lillerud, S. Kolboe, I.M. Dahl, *J. Catal.*, 241 (2006) 243-254.

(94) B.P.C. Hereijgers, F. Bleken, M.H. Nilsen, S. Svelle, K.P. Lillerud, M. Bjørgen, B.M. Weckhuysen, U. Olsbye, *J. Catal.*, 264 (2009) 77-87.

(95) F. Bleken, M. Bjørgen, L. Palumbo, S. Bordiga, S. Svelle, K.P. Lillerud, U. Olsbye, *Top. Catal.*, 52 (2009) 218-228.

(96) F. Bleken, W. Skistad, K. Barbera, M. Kustova, S. Bordiga, P. Beato, K.P. Lillerud, S. Svelle, U. Olsbye, *Phys. Chem. Chem. Phys.*, 13 (2011) 2539-2549.

(97) M. Bjørgen, U. Olsbye, S. Svelle, S. Kolboe, *Catal. Lett.*, 93 (2004) 37-40.

(98) M. Bjørgen, S. Kolboe, *Appl. Catal., A*, 225 (2002) 285-290.

(99) K. Barbera, F. Bonino, S. Bordiga, T.V.W. Janssens, P. Beato, *J. Catal.*, 280 (2011) 196-205.

(100) D.S. Wragg, M.G. O'Brien, F.L. Bleken, M. Di Michiel, U. Olsbye, H. Fjellvag, *Angew. Chem., Int. Ed.*, 51 (2012) 7956-7959.

(101) J.F. Haw, W.G. Song, D.M. Marcus, J.B. Nicholas, *Acc. Chem. Res.*, 36 (2003) 317-326.

(102) S. Kolboe, L. Kubelkova, W.O. Haag, J.J. Rooney, A.A. Tsyganenko, W.K. Hall, A. Bielanski, H. Schulz, *Stud. Surf. Sci. Catal.*, 75 (1993) 449-461.

(103) J.Z. Li, Y. Qi, Z.M. Liu, G.Y. Liu, D.Z. Zhang, *Catal. Lett.*, 121 (2008) 303-310.

(104) Z.M. Cui, Q. Liu, W.G. Song, L.J. Wan, *Angew. Chem., Int. Ed.*, 45 (2006) 6512-6515.

(105) Z.M. Cui, Q. Liu, S.W. Baint, Z. Ma, W.G. Song, *J. Phys. Chem. C*, 112 (2008) 2685-2688.

(106) Z.M. Cui, Q. Liu, Z. Ma, S.W. Bian, W.G. Song, *J. Catal.*, 258 (2008) 83-86.

(107) S. Svelle, P.O. Rønning, S. Kolboe, *J. Catal.*, 224 (2004) 115-123.

(108) Ø. Mikkelsen, S. Kolboe, *Microporous Mesoporous Mater.*, 29 (1999) 173-184.

(109) F.L. Bleken, T.V.W. Janssens, S. Svelle, U. Olsbye, *Microporous Mesoporous Mater.*, 164 (2012) 190-198.

(110) H. Schulz, *Catal. Today*, 154 (2010) 183-194.

(111) M. Kaarsholm, F. Joensen, J. Nerlov, R. Cenni, J. Chaouki, G.S. Patience, *Chem. Eng. Sci.*, 62 (2007) 5527-5532.

(112) J.Z. Li, Y.X. Wei, G.Y. Liu, Y. Qi, P. Tian, B. Li, Y.L. He, Z.M. Liu, *Catal. Today*, 171 (2011) 221-228.

(113) J.Z. Li, Y.X. Wei, Y. Qi, P. Tian, B. Li, Y.L. He, F.X. Chang, X.D. Sun, Z.M. Liu, *Catal. Today*, 164 (2011) 288-292.

(114) N.Y. Chen, W.E. Garwood, *J. Catal.*, 52 (1978) 453-458.

(115) R.F. Li, W.B. Fan, J.H. Ma, B.B. Fan, J.H. Cao, *Zeolites*, 15 (1995) 73-76.

(116) W.B. Fan, R.F. Li, B.B. Fan, J.H. Ma, J.H. Cao, *Appl. Catal., A*, 143 (1996) 299-308.

(117) P.J. Hogan, T.V. Whittam, J.J. Birtill, A. Stewart, *Zeolites*, 4 (1984) 275-279.

(118) W. Huybrechts, G. Vanbutsele, K.J. Houthoofd, F. Bertinchamps, C.L.S. Narasimhan, E.M. Gaigneaux, J.W. Thybaut, G.B. Marin, J.F.M. Denayer, G.V. Baron, P.A.A. Jacobs, J.A. Martens, *Catal. Lett.*, 100 (2005) 235-242.

(119) N. Katada, H. Igi, J.H. Kim, M. Niwa, *J. Phys. Chem. B*, 101 (1997) 5969-5977.

(120) K. Moller, T. Bein, *Microporous Mesoporous Mater.*, 143 (2011) 253-262.

(121) D. Verboekend, A.M. Chabaneix, K. Thomas, J.P. Gilson, J. Pérez-Ramírez, *CrystEngComm*, 13 (2011) 3408-3416.

(122) L. Rodríguez-González, F. Hermes, M. Bertmer, E. Rodríguez-Castellón, A. Jiménez-López, U. Simon, *Appl. Catal., A*, 328 (2007) 174-182.

(123) J. Kim, M. Choi, R. Ryoo, *J. Catal.*, 269 (2010) 219-228.

(124) S. Ferdov, Z. Lin, R.A.S. Ferreira, *Chem. Lett.*, 37 (2008) 100-101.

(125) K. Hayasaka, D. Liang, W. Huybrechts, B.R. De Waele, K.J. Houthoofd, P. Eloy, E.M. Gaigneaux, G. van Tendeloo, J.W. Thybaut, G.B. Marin, J.F.M. Denayer, G.V. Baron, P.A. Jacobs, C.E.A. Kirschhock, J.A. Martens, *Chem. Eur. J.*, 13 (2007) 10070-10077.

(126) Q.H. Xu, Y.J. Gong, W.J. Xu, J. Xu, F. Deng, T. Dou, *J. Colloid Interface Sci.*, 358 (2011) 252-260.

(127) W. Souverijns, W. Verrelst, G. Vanbutsele, J.A. Martens, P.A. Jacobs, *J. Chem. Soc., Chem. Commun.*, (1994) 1671-1672.

(128) S. Lawton, M.E. Leonowicz, R. Partridge, P. Chu, M.K. Rubin, *Microporous Mesoporous Mater.*, 23 (1998) 109-117.

(129) R. Ravishankar, D. Bhattacharya, N.E. Jacob, S. Sivasanker, *Microporous Materials*, 4 (1995) 83-93.

(130) S. Inagaki, K. Kamino, M. Hoshino, E. Kikuchi, M. Matsukata, *Bull. Chem. Soc. Jpn.*, 77 (2004) 1249-1254.

(131) M. Choi, K. Na, J. Kim, Y. Sakamoto, O. Terasaki, R. Ryoo, *Nature*, 461 (2009) 246-249.

(132) A.J. Marchi, G.F. Froment, *Appl. Catal.*, 71 (1991) 139-152.

(133) D. Chen, H.P. Rebo, A. Grønvold, K. Moljord, A. Holmen, *Microporous Mesoporous Mater.*, 35-6 (2000) 121-135.

(134) D. Chen, H.P. Rebo, K. Moljord, A. Holmen, *Ind. Eng. Chem. Res.*, 36 (1997) 3473-3479.

(135) T.V.W. Janssens, *J. Catal.*, 264 (2009) 130-137.

(136) D.J. Earl, M.W. Deem, *Ind. Eng. Chem. Res.*, 45 (2006) 5449-5454.

(137) A.C. Gujar, G.L. Price, *Microporous Mesoporous Mater.*, 54 (2002) 201-205.

(138) R. Docherty, G. Clydesdale, K.J. Roberts, P. Bennema, *J. Phys. D: Appl. Phys.*, 24 (1991) 89-99.

(139) A. Katerinopoulou, T. Balic-Zunic, L.F. Lundegaard, *J. Appl. Crystallogr.*, 45 (2012) 22-27.

(140) W. Zhang, Y. Wu, J. Gu, H. Zhou, J. Wang, *Mater. Res. Bull.*, 46 (2011) 1451-1454.

(141) L.R. Martens, J.P. Verduijn, G.M. Mathys, *Catal. Today*, 36 (1997) 451-460.

(142) A.E.W. Beers, J.A. van Bokhoven, K.M. de Lathouder, F. Kapteijn, J.A. Moulijn, *J. Catal.*, 218 (2003) 239-248.

(143) A. Gola, B. Rebours, E. Milazzo, J. Lynch, E. Benazzi, S. Lacombe, L. Delevoye, C. Fernandez, *Microporous Mesoporous Mater.*, 40 (2000) 73-83.

(144) L. Yingca, J. Mingyang, S. Yaojun, W. Tailiu, W. Liping, F. Lun, *J. Chem. Soc., Faraday Trans.*, 92 (1996) 1647-1651.

Appendix

Paper I

Shape-Selective Conversion of Methanol to Hydrocarbons Over 10-Ring Unidirectional-Channel Acidic H-ZSM-22

S. Teketel, S. Svelle, K. P. Lillerud, U. Olsbye.

ChemCatChem 1 (2009) 78-81

Paper II

Selectivity Control through Fundamental Mechanistic Insight in the Conversion of Methanol to Hydrocarbons over Zeolites

S. Teketel, U. Olsbye, K. P. Lillerud, P. Beato, S. Svelle.

Microporous Mesoporous Mater. 136 (2010) 33-41.

Paper III

Shape Selectivity in the Conversion of Methanol to Hydrocarbons: The Catalytic Performance of One-Dimensional 10-Ring Zeolites: ZSM-22, ZSM-23, ZSM-48, and EU-1

S. Teketel, W. Skistad, S. Benard, U. Olsbye, K. P. Lillerud, P. Beato, S. Svelle.

ACS Catal. 2 (2012) 26-37

Paper IV

Morphology Induced Shape Selectivity in Zeolite Catalysis

S. Teketel, L. F. Lundegaard, U. Olsbye, K. P. Lillerud, P. Beato, S. Svelle.

Preliminary manuscript (2012)

Paper V

Co-conversion of Methanol and Light Alkenes to Hydrocarbons over Acidic Zeolite Catalyst H-ZSM-22: Simulated Recycle of Non-Gasoline Products

S. Teketel; U. Olsbye, K. P. Lillerud, P. Beato, S. Svelle

Preliminary manuscript (2012)